Spectral properties of Fluid Structure Interaction pressure/stress waves in liquid filled pipes

Alexandre Bayle, Franck Plouraboue

Highlights

Spectral properties of Fluid Structure Interaction pressure/stress waves in liquid filled pipes

A.Bayle, F.Plouraboué

- Research highlight 1: Explicit analytical solutions for Fluid Structure Interaction (FSI) waves propagation occurring in liquid filled pipes are developed
- Research highlight 2: Convoluted behavior of time dependent solutions is spelled out.
- Research highlight 3: These theoretical solutions perfectly match with previous published numerical results
- Research highlight 4: The hereby theoretical framework applies to a broad range of boundary conditions
- Research highlight 5: The spectrum sensitivity is theoretically and numerically investigated.

Spectral properties of Fluid Structure Interaction pressure/stress waves in liquid filled pipes

A.Bayle, F.Plouraboué

[a]*Institut de Mécanique des Fluides de Toulouse, IMFT, Université de Toulouse, CNRS, Toulouse, 31400, France*

Abstract

We hereby develop a theoretical framework for analyzing Fluid Structure Interaction (FSI) waves propagation occurring in liquid filled pipes to manage a large family set of boundary conditions (e.g. junctions coupling effects). A self-adjoint operator theory framework leads to the analytical derivation of a transcendental equations for operator's spectrum. The latter provides the system's natural resonant frequencies as well as permit to find the discrete mode orthogonal basis decomposition. This theoretical framework also permits to demonstrate that the spectrum is uniquely composed into simple eigenvalues enabling explicit time-domain solutions from inverse-Laplace transform. The analysis is directly conducted in the time-domain but the obtained spectrum also applies to Fourier transformed frequency analysis. The obtained analytical solutions are successfully confronted with numerical simulation obtained using the Method of characteristic (MOC) for the same four equations (FSI) model on the very same configurations. The spectrum sensitivity matrix is also explicitly evaluated.

Keywords: Fluid Structure Interaction (FSI), Liquid filled pipes, Junction coupling, Operator's spectrum, Time domain solution, Method of characteristics (MOC)

1. Introduction

Wave propagation in liquid-filled pipe systems have been investigated for a long time [1, 2, 3, 4, 5, 6, 7] to cite only a few, possibly seminal, contributers. The phenomenology is now well understood as fully discussed in exhaustive and sagacious review papers [8, 9, 10]. Fluid Structure Interaction

(FSI) arising between pressure/stress propagation have been recognized as one major modeling pathway, leading to four coupled hyperbolic equations in the case of axi-symmetric compressive planar waves modes propagation [5, 11, 12, 7, 13]. The long wavelength approximation is a widely established and validated framework [3, 14, 15, 7]. It permits to neglect secondary FSI effects associated with rotatory vibration modes or radial inertia (e.g. bending, twisting, etc..), the analysis of which needs a more complex set of equations. Considering an averaged formulation both in solid and fluid for mass and momentum conservation equations, [7] derive a set of four coupled hyperbolic equations highlighting the overriding role of the Poisson's coupling effects, namely the axial transmission of the radial stresses and strains via the Poisson's modulus, on the whole dynamic. In [16] two other major coupling mechanisms were spelled out: (i) the junction occurring at edge conditions and, (ii) the friction coupling resulting from viscous effects in boundary layers and/or pipe's supports. Whereas (i) is precisely analyzed in this study, on the contrary, (ii) is not considered. Pipe's support coupling effects has nevertheless been thoroughly analyzed in [6, 17, 18].

Recent and active motivations to analyze the FSI vibrations in pipes lies from the use of water-hammer waves in defect/leak detection and localization [19, 20, 21, 22, 23]. Since in common practice "localized" pipe anomaly, such as a leak and a discrete blockage leads to a modification of the Fourier peaks of the signal, a spectral-based diagnostic signal processing has been sough for [19, 21, 22, 23]. In this context, the ability to obtain an explicit derivation of the traveling waves system spectral properties can pave the way to elaborate spectral diagnostic signal processing strategies among which the spectral sensitivity matrix is a central one [24, 25]. As spectral sensitivity matrix is a time-consuming and noise-sensitive quantity, a purely numerical estimate of this quantity, e.g. based upon finite-difference estimate, is sometimes not precise enough or too demanding (in case of high-dimensionality of parameter space). This is why it is either interesting to lower the parameter space dimensions and/or to find analytical estimate of this spectral sensitivity matrix, as performed here. Many contributions relying on the Laplace/frequency-domain numerical resolution of the FSI four equations using transfer matrix method (TMM) can be found [9, 26, 27, 28, 29, 30, 20]. Nevertheless, to our knowledge, no fully explicit time-domain solutions nor explicit spectrum have been previously obtained except in [31], which has ignored Poisson's coupling and therefore (FSI) interactions. In the following, we thereby focus on developing a new analytical framework using operator's

theory, for pressure/stress wave operator. We derive a straightforward real transcendental equation for the spectrum and successfully spelled out an orthogonal projection basis for the uncoupled diagonalized wave operator. The separation of variables technique is used to handle the derivation of a pressure-stress solution in time-domain (a Fourier transform may thereafter easily be managed, if required, to find the corresponding frequency domain solution). The paper is organized as follow. Section 2.1 describes the dimensionless constitutive (FSI) 4-equations model, boundary conditions sets, parametric description, proper wave dimensional and dimensionless velocity propagation, and the resulting diagonalized 2-waves equations reminiscent of [28]'s solution strategy. Section 3 provides the theoretical framework defining the self-adjoint operator for the separable waves solutions decomposition. Section 4 illustrates the comparison between the obtained analytical solutions and previously published numerical or theoretical results for specific sets of boundary conditions. Section 5 then provides the spectrum sensitivity matrix for each boundary condition set.

2. Governing equations

2.1. Dimensionless constitutive model

Let us consider a cylindrical tube having inner radius R_0, wall thickness e, and length L, which defines the following aspect and geometrical parameters

$$\alpha = \frac{e}{R_0} \quad \text{, and,} \quad \epsilon = \frac{R_0}{L}. \tag{1}$$

The tube is supposed to be entirely filled with a fluid having density ρ_f, bulk modulus K, perturbed pressure P^* and velocity W^*. Considering low-Mach waves, the fluid density is considered as constant and equal to the reference density ρ_f as in [32, 33]. The elastic solid response is associated with Young's modulus, E, Poisson's modulus ν_s, perturbed axial stress, σ^*, perturbed axial strain ζ^*, and density ρ_s supposed constant. [7] derived the classical pulse wave speed within the fluid, c_p, distinct from the elastic pulse wave speed within the solid, c_s, the ratio of which is denoted $\mathcal{C}_s$

$$c_p^2 = \frac{\frac{K}{\rho_f}}{1 + \frac{2K}{\alpha E}\left(\frac{2(1-\nu_s^2)}{2+\alpha} + \alpha(1+\nu_s)\right)}, \quad c_s^2 = \frac{E}{\rho_s}, \quad \mathcal{C}_s = \frac{c_s}{c_p}. \tag{2}$$

The coupled system is furthermore described through the dimensionless density ratio

$$\mathcal{D} = \frac{\rho_f}{\rho_s}, \tag{3}$$

so that the dimensionless FSI four-equations derived in [7] achieves as follows

$$\begin{aligned}
\partial_\tau W &= -\partial_Z P, && (4)\\
\partial_\tau P + \partial_Z W &= 2\alpha\nu_s \partial_Z \dot{\zeta}, && (5)\\
\partial_\tau \dot{\zeta} &= \frac{\mathcal{D}}{\alpha}\partial_Z \sigma, && (6)\\
\partial_\tau \sigma - \frac{\alpha \mathcal{C}_s^2}{\mathcal{D}}\partial_Z \dot{\zeta} &= \frac{2\nu_s}{\alpha(2+\alpha)}\partial_\tau P. && (7)
\end{aligned}$$

where W, P, $\dot{\zeta}$, σ are dimensionless quantities referring to the fluid longitudinal velocity, the fluid pressure, the longitudinal solid deformation velocity and the longitudinal stress, respectively. The physical time t is scaled on the advective fluid pulse one, i.e. $\tau \equiv \frac{c_p}{L}t$, whilst the longitudinal coordinate z is scaled on the tube's length, i.e. $z \equiv LZ$. More details on the hereby dimensionless derivation is provided in Appendix B. (4)-(7) represents a set of two coupled hyperbolic equations. While the first part (4)-(5) is associated with the acoustic waves propagation in the fluid, the second part (6)-(7) describes the propagation of axial compressible waves in the solid tube. Poisson's coupling is highlighted by the presence of the Poisson's modulus in both source terms of (5) and (7).

It is noteworthy to point-out that (4)-(7) are the leading order contributions regarding small parameter ϵ [34]. [3, 35, 14] in-depth analyzed the secondary (FSI) interactions occurring in liquid filled pipe systems, revealing their significant impact at very high-frequencies only, the cut-off of which f_{Kc}, is known as the Korteweg's stop band, [36]

$$f_{Kc} = \frac{\mathcal{C}_s}{\epsilon} f_0 \quad \text{, with,} \quad f_0 = \frac{c_p}{2\pi L}. \tag{8}$$

For $f_{Kc} > f > f_0$, the axial dynamics prevails over the radial one and despite simplifications (4)-(7) is relevant to investigate several configurations [37, 7, 38, 39]. This frequency cut-off f_{Kc} nevertheless stands as a frequency limitation of the proposed analysis and will be thereafter discussed. Last but not least, it is known from [31, 40] that viscous shear dissipation occurring at the fluid and solid interface may have a significant impact on the coupling

dynamic. Even though of physical interest, this issue is herein discarded but in-depth analyzed in [41]. Considering the acoustic framework for the fluid whilst using the linearity of the FSI-governing equations, only the perturbed component of the physical field are investigated so that the initial conditions are

$$\mathbf{Y}(Z,0) = \partial_\tau \mathbf{Y}(Z,0) = \mathbf{0}, \tag{9}$$

with $\mathbf{Y}(Z,\tau)$ a four column vector,

$$\mathbf{Y}(Z,\tau) = \Big(P(Z,\tau), \sigma(Z,\tau), W(Z,\tau), \dot{\zeta}(Z,\tau)\Big)^T, \tag{10}$$

where subscript T holds for the conjugate transpose.

2.2. Vectorial two-waves system of FSI four-equations

The four coupled hyperbolic (4)-(7) are hereby re-organized to bring-up a d'Alembert operator upon the time-space dependent variable $\mathbf{Y}$

$$\left(\partial_\tau^2 - \mathbf{C}_\mathbf{Y}^2 \partial_Z^2\right) \mathbf{Y}(Z,\tau) = \mathbf{0}, \tag{11}$$

where,

$$\mathbf{C}_\mathbf{P}^2 = \begin{pmatrix} 1 & 2\nu_s\mathcal{D} \\ \frac{2\nu_s}{\alpha(2+\alpha)} & \frac{4\nu_s^2\mathcal{D}}{\alpha(2+\alpha)} + \mathcal{C}_s^2 \end{pmatrix}, \quad \mathbf{C}_\mathbf{W}^2 = \begin{pmatrix} 1 & -2\alpha\nu_s \\ -\frac{2\nu_s\mathcal{D}}{\alpha^2(2+\alpha)} & \frac{4\nu_s^2\mathcal{D}}{\alpha(2+\alpha)} + \mathcal{C}_s^2 \end{pmatrix} \tag{12}$$

and

$$\mathbf{C}_\mathbf{Y}^2 = \begin{pmatrix} \mathbf{C}_\mathbf{P}^2 & \mathbf{0} \\ \mathbf{0} & \mathbf{C}_\mathbf{W}^2 \end{pmatrix}. \tag{13}$$

Eigenvalues of the $\mathbf{C}_\mathbf{P}^2$ and $\mathbf{C}_\mathbf{W}^2$ matrices correspond to coupled vibrating modes wave speeds propagation. Both matrices have identical eigenvalues, $c_\pm^2$, the solutions of the polynomial characteristic problem

$$c_\pm^4 - \left[1 + \mathcal{C}_s^2 + \frac{4\nu_s^2\mathcal{D}}{\alpha(2+\alpha)}\right] c_\pm^2 + \mathcal{C}_s^2 = 0, \tag{14}$$

then achieves as follows

$$c_\pm^2 = \frac{1 + \mathcal{C}_s^2 + \frac{4\nu_s^2\mathcal{D}}{\alpha(2+\alpha)} \pm \sqrt{\left(1 + \mathcal{C}_s^2 + \frac{4\nu_s^2\mathcal{D}}{\alpha(2+\alpha)}\right)^2 - 4\mathcal{C}_s^2}}{2}. \tag{15}$$

(15) stands for the dimensionless version of coupled wave speed modes derived in [6, 7, 28]. The choice for denoting $\mathbf{C}^2_{\mathbf{P}}$ and $\mathbf{C}^2_{\mathbf{W}}$ matrices with a square as well as its eigenvalues $c^2_{\pm}$, now becomes clear since $c_{\pm}$ describes the wave speed of each propagating mode, each governed by their specific D'Alembert operator. Dimensionless wave speed, c_{-}, has a value close to one, whilst c_{+} is found close to $\mathcal{C}_s$. In Appendix E a systematic asymptotic analysis provides the Poisson coupling corrections to these quantities as $\nu_s \ll 1$. The mode c_{-} is thus associated with the fluid pulse mode while, c_{+} is associated with the solid elastic one. Furthermore, it is noteworthy to point-out that the negative mode of (15) is always real in the Korteweg's frequency range since for real $\mathcal{C}_s^2$ parameter

$$\left(1-\mathcal{C}_s^2\right)^2 > -\frac{4\nu_s^2\mathcal{D}}{\alpha(2+\alpha)}\left[\frac{4\nu_s^2\mathcal{D}}{\alpha(2+\alpha)}+2\left(1+\mathcal{C}_s^2\right)\right], \tag{16}$$

is always satisfied. This property nevertheless vanishes as $f > f_{Kc}$, in which case the radial contributions leads to a dispersive waves, the propagating velocity of which can be complex [3, 36]. The D'Alembert wave propagation operator is hereby regarded within the diagonal base of $\mathbf{C}^2_{\mathbf{Y}}$ as classically performed in coupled hyperbolic systems [21, 28, 29]. The transition matrices $\mathbf{\Pi_Y}$ of the diagonal base change can easily be deduced from $\mathbf{C}^2_{\mathbf{P}}$ and $\mathbf{C}^2_{\mathbf{W}}$ eigenvectors

$$\mathbf{\Pi_Y}=\begin{pmatrix}\mathbf{\Pi_P} & \mathbf{0}\\ \mathbf{0} & \mathbf{\Pi_W}\end{pmatrix}, \mathbf{\Pi_P}=\begin{pmatrix}\frac{2\nu_s\mathcal{D}}{c_-^2-1} & \frac{2\nu_s\mathcal{D}}{c_+^2-1}\\ 1 & 1\end{pmatrix}, \mathbf{\Pi_W}=\begin{pmatrix}\frac{2\alpha\nu_s}{c_-^2-1} & \frac{2\alpha\nu_s}{c_+^2-1}\\ 1 & 1\end{pmatrix}, \tag{17}$$

such as the transition relations

$$\boldsymbol{\mathcal{C}}^2_{\boldsymbol{\mathcal{Y}}}=\mathbf{\Pi}_{\mathbf{Y}}^{-1}\mathbf{C}^2_{\mathbf{Y}}\mathbf{\Pi_Y}=\begin{pmatrix}\boldsymbol{\mathcal{C}}^2_{\boldsymbol{\mathcal{P}}} & \mathbf{0}\\ \mathbf{0} & \boldsymbol{\mathcal{C}}^2_{\boldsymbol{\mathcal{W}}}\end{pmatrix}, \text{ and, } \boldsymbol{\mathcal{Y}}=\mathbf{\Pi}_{\mathbf{Y}}^{-1}\mathbf{Y}, \tag{18}$$

where

$$\boldsymbol{\mathcal{C}}^2_{\boldsymbol{\mathcal{P}}}=\mathbf{\Pi}_{\boldsymbol{\mathcal{P}}}^{-1}\mathbf{C}^2_{\mathbf{P}}\mathbf{\Pi}_{\boldsymbol{\mathcal{P}}}=\begin{pmatrix}c_-^2 & 0\\ 0 & c_+^2\end{pmatrix}, \text{ and, } \boldsymbol{\mathcal{C}}^2_{\boldsymbol{\mathcal{W}}}=\mathbf{\Pi}_{\boldsymbol{\mathcal{W}}}^{-1}\mathbf{C}^2_{\mathbf{W}}\mathbf{\Pi}_{\boldsymbol{\mathcal{W}}}=\begin{pmatrix}c_-^2 & 0\\ 0 & c_+^2\end{pmatrix}. \tag{19}$$

The dimensionless wave-equations system (11) and its initial conditions (9) expressed in the eigenvector base finally reads

$$\left(\partial_\tau^2-\boldsymbol{\mathcal{C}}^2_{\boldsymbol{\mathcal{Y}}}\partial_Z^2\right)\boldsymbol{\mathcal{Y}} = \mathbf{0}, \tag{20}$$

$$\boldsymbol{\mathcal{Y}}(Z,0)=\partial_\tau\boldsymbol{\mathcal{Y}}(Z,0) = \mathbf{0}. \tag{21}$$

The operator (11) diagonalization has indeed simplified the mode propagation now described by two independent D'Alembert propagating waves but obviously not suppressed their coupling. The coupling is now recast in the resulting upstream and downstream boundary conditions. Boundary conditions for $\boldsymbol{\mathcal{Y}}$ can be deduced from the mechanical boundary conditions associated with $\mathbf{Y}$ using change-basis relations (19). For the sake of notation simplification let us introduce four 4×4 matrices $\boldsymbol{\mathcal{N}}$, $\boldsymbol{\mathcal{M}}$, $\boldsymbol{\mathcal{Q}}$, $\boldsymbol{\mathcal{R}}$ and $\boldsymbol{\mathcal{S}}(\tau)$ a eight-dimensional column vector. Boundary conditions can formally be written as a rectangular 8×16 linear system

$$\begin{pmatrix} \boldsymbol{\mathcal{N}} & \boldsymbol{\mathcal{M}} & \mathbf{0} & \mathbf{0} \\ \mathbf{0} & \mathbf{0} & \boldsymbol{\mathcal{Q}} & \boldsymbol{\mathcal{R}} \end{pmatrix}_{(8\times16)} \begin{pmatrix} \boldsymbol{\mathcal{Y}}(0,\tau) \\ \partial_Z \boldsymbol{\mathcal{Y}}(0,\tau) \\ \boldsymbol{\mathcal{Y}}(1,\tau) \\ \partial_Z \boldsymbol{\mathcal{Y}}(1,\tau) \end{pmatrix}_{(16\times1)} = \boldsymbol{\mathcal{S}}_{(8\times1)}(\tau). \tag{22}$$

Specifics set of boundary conditions are later on considered in section 4. The resolution of this vector waves equation is usually handled by Laplace transform, combined with usual transfer matrix method [28, 9, 29]. Some analytical difficulties are sometimes nevertheless encountered when performing the inverse Laplace transform. Thereafter a new analytical derivation for solution of (20), having initial conditions (21) and spatial boundary conditions (22), relying on variable separation, spectral analysis and self-adjoint operator theory is proposed.

3. Analytical framework

3.1. Self-adjoint operator theory

Let us define the operator $\mathcal{H}$, acting on the square-integrable real four dimensional column vector field $\boldsymbol{\Psi}(Z)$,

$$\forall \boldsymbol{\Psi}(Z) \in L^4(\mathbb{R}) \times L^4(\mathbb{R}), \quad \boldsymbol{\Psi}(Z) \to \mathcal{H}\boldsymbol{\Psi}(Z) = \boldsymbol{\mathcal{C}}_{\boldsymbol{\mathcal{Y}}}^2 \cdot \partial_Z^2 \boldsymbol{\Psi}(Z), \tag{23}$$

with the homogeneous associated set of spatial boundary conditions,

$$\begin{pmatrix} \boldsymbol{\mathcal{N}} & \boldsymbol{\mathcal{M}} & \mathbf{0} & \mathbf{0} \\ \mathbf{0} & \mathbf{0} & \boldsymbol{\mathcal{Q}} & \boldsymbol{\mathcal{R}} \end{pmatrix}_{(8\times16)} \begin{pmatrix} \boldsymbol{\Psi}(0) \\ \partial_Z \boldsymbol{\Psi}(0) \\ \boldsymbol{\Psi}(1) \\ \partial_Z \boldsymbol{\Psi}(1) \end{pmatrix}_{(16\times1)} = \mathbf{0}. \tag{24}$$

Let us set up the general scalar product,

$$\forall \boldsymbol{\Psi}, \boldsymbol{\Psi}^{'} \in L^4(\mathbb{R}) \times L^4(\mathbb{R}), \quad \langle \boldsymbol{\Psi}^{'}, \boldsymbol{\Psi} \rangle = \sum_{j=1}^{4} \eta_j \int_0^1 \Psi_j^{'}(Z) \Psi_j(Z) dZ, \tag{25}$$

with $j = 1, 2, 3, 4$ referring to the j^{th} components of vector $\boldsymbol{\eta} \equiv (\eta_1, \eta_2, \eta_3, \eta_4) \in \mathbb{R}^4$, a yet unknown real vector which is adapted to each specific problem. Invoking the definition of $\mathcal{H}$ in (23), the search for self-adjoint condition for operator $\mathcal{H}$, equipped with scalar product (25), performing a double integration by parts leads to

$$\begin{aligned} \langle \mathcal{H}\boldsymbol{\Psi}, \boldsymbol{\Psi}^{'} \rangle = \langle \boldsymbol{\mathcal{C}}_{\boldsymbol{\mathcal{Y}}}^2 \cdot \partial_Z^2 \boldsymbol{\Psi}, \boldsymbol{\Psi}^{'} \rangle = \langle \boldsymbol{\Psi}, \boldsymbol{\mathcal{C}}_{\boldsymbol{\mathcal{Y}}}^2 \cdot \partial_Z^2 \boldsymbol{\Psi}^{'} \rangle + \\ \sum_{j=1}^{4} \eta_j c_j^2 \left(\left[\partial_Z \Psi_j(Z) \Psi_j^{'}(Z) - \Psi_j(Z) \partial_Z \Psi_j^{'}(Z) \right]_0^1 \right), \end{aligned} \tag{26}$$

where c_j^2 are the j^{th} diagonal terms of $\boldsymbol{\mathcal{C}}_{\boldsymbol{\mathcal{Y}}}^2$. Self-adjoint property $\langle \mathcal{H}\boldsymbol{\Psi}, \boldsymbol{\Psi}^{'} \rangle = \langle \boldsymbol{\Psi}, \mathcal{H}\boldsymbol{\Psi}^{'} \rangle$, is thus obtained from condition

$$\sum_{j=1}^{4} \eta_j c_j^2 \left[\partial_Z \Psi_j(Z) \Psi_j^{'}(Z) - \Psi_j(Z) \partial_Z \Psi_j^{'}(Z) \right]_0^1 = 0. \tag{27}$$

In the following, the scalar-product weight parameter $\boldsymbol{\eta}$ is adjusted with given boundary conditions set so as to ensure relation eq(27), and thus self-adjointness.

3.2. Eigenfunction base and spectrum condition

The self-adjoint operator $\mathcal{H}$ spectrum $\mathcal{S}_{\mathcal{P}}$, is composed of real discrete eigenvalues having a related discrete orthogonal basis [42]. This property obviously remains for frequency up to the Korteweg's band stop. Denoting $-\lambda_k^2$ the k^{th} eigenvalue, then being real negative in accordance with the well known eigenvalues of the Laplacian , $\boldsymbol{\Phi}_k$ its related eigen-function, the eigenvalue problem reads

$$\mathcal{H}\boldsymbol{\Phi}_k(Z) = -\lambda_k^2 \boldsymbol{\Phi}_k(Z), \tag{28}$$

so that using (23), one gets

$$\partial_Z^2 \boldsymbol{\Phi}_k(Z) = -\lambda_k^2 \boldsymbol{\mathcal{C}}_{\boldsymbol{\mathcal{Y}}}^{-2} \boldsymbol{\Phi}_k(Z), \tag{29}$$

where we have introduced notation $\boldsymbol{\mathcal{C}}_{\boldsymbol{\mathcal{Y}}}^{-2} \equiv [\boldsymbol{\mathcal{C}}_{\boldsymbol{\mathcal{Y}}}^{2}]^{-1}$ for the inverse of matrix $\boldsymbol{\mathcal{C}}_{\boldsymbol{\mathcal{Y}}}^{2}$ defined in (18). The solution of (29) then achieves as follows

$$\begin{pmatrix} \boldsymbol{\Phi}_k(Z) \\ \partial_Z \boldsymbol{\Phi}_k(Z) \end{pmatrix} = \boldsymbol{\mathcal{T}}_k(Z) \begin{pmatrix} \boldsymbol{\Phi}_k(0) \\ \partial_Z \boldsymbol{\Phi}_k(0) \end{pmatrix}_{(8\times 1)}, \tag{30}$$

with

$$\boldsymbol{\mathcal{T}}_k(Z) = \begin{pmatrix} \partial_Z \mathbf{T}(Z) & \mathbf{T}(Z) \\ \partial_Z^2 \mathbf{T}(Z) & \partial_Z \mathbf{T}(Z) \end{pmatrix}, \quad \mathbf{T}(Z) = \begin{pmatrix} \mathbf{T}_s(Z) & \mathbf{0} \\ \mathbf{0} & \mathbf{T}_s(Z) \end{pmatrix}, \tag{31}$$

and

$$\mathbf{T}_s(Z, \lambda_k) = \frac{1}{\lambda_k} \begin{pmatrix} c_- \sin\left(\frac{\lambda_k Z}{c_-}\right) & 0 \\ 0 & c_+ \sin\left(\frac{\lambda_k Z}{c_+}\right) \end{pmatrix}. \tag{32}$$

This formulation is a modal time-domain version of the popular transfer matrix method, (TMM), developed in the frequency domain for coupled hyperbolic problems in [9, 21, 22, 26, 27, 28, 29, 30] but for the adaption to the need for a Laplacian operator of two boundary conditions to be specified. Combining (30) and (32) in boundary condition set (24) provides the following linear condition to be fulfilled by mode amplitudes $[\boldsymbol{\Phi}_k(0), \partial_Z \boldsymbol{\Phi}_k(0)]$

$$\begin{pmatrix} \boldsymbol{\mathcal{N}} & \boldsymbol{\mathcal{M}} \\ \boldsymbol{\mathcal{Q}} \partial_Z \mathbf{T}(1) + \boldsymbol{\mathcal{R}} \partial_Z^2 \mathbf{T}(1) & \boldsymbol{\mathcal{Q}} \mathbf{T}(1) + \boldsymbol{\mathcal{R}} \partial_Z \mathbf{T}(1) \end{pmatrix} \begin{pmatrix} \boldsymbol{\Phi}_k(0) \\ \partial_Z \boldsymbol{\Phi}_k(0) \end{pmatrix} = \mathbf{0}. \tag{33}$$

The trivial zero solution of (33) being irrelevant, the non-trivial solution necessitates a one-dimensional non-empty kernel of (33)'s matrix, i.e. a zero eigenvalue of the matrix acting on $[\boldsymbol{\Phi}_k(0), \partial_Z \boldsymbol{\Phi}_k(0)]$ vector. This condition is equivalent to set a zero determinant of (33)'s matrix, i.e.

$$\begin{vmatrix} \boldsymbol{\mathcal{N}} & \boldsymbol{\mathcal{M}} \\ \boldsymbol{\mathcal{Q}} \partial_Z \mathbf{T}(1) + \boldsymbol{\mathcal{R}} \partial_Z^2 \mathbf{T}(1) & \boldsymbol{\mathcal{Q}} \mathbf{T}(1) + \boldsymbol{\mathcal{R}} \partial_Z \mathbf{T}(1) \end{vmatrix} = \mathbf{0}. \tag{34}$$

(34) is met for specific values of λ_k, providing the spectrum $\mathcal{S}_{\mathcal{P}}$ of operator $\mathcal{H}$. It leads to a transcendental equation for λ_k specific to each boundary condition set, to be computed numerically, as done in section 4. The spectrum provides each resonant frequency of the system, which should lie in the frequency range given in (8), i.e. $\lambda_k \in [-f_{Kc}/f_0, f_{Kc}/f_0]$. It remains to determine the modal-dependent amplitudes of $\boldsymbol{\Phi}_k(Z)$. From (34) one can realize that the amplitude vector $[\boldsymbol{\Phi}_k(0), \partial_Z \boldsymbol{\Phi}_k(0)]$ is defined up to any arbitrary multiplicative constant, as the kernel of (33)'s matrix is non-empty.

Hence, among the eight amplitude parameters of eight-dimensional vector $[\boldsymbol{\Phi}_k(0), \partial_Z \boldsymbol{\Phi}_k(0)]$, one can be kept to any arbitrary value, which is equivalent to chose a unitary eigenfunction $\boldsymbol{\Phi}_k(Z)$ such as

$$\begin{pmatrix} \boldsymbol{\Phi}_k(Z) \\ \partial_Z \boldsymbol{\Phi}_k(Z) \end{pmatrix} = \frac{1}{\|\tilde{\boldsymbol{\Phi}}_k(Z)\|} \begin{pmatrix} \tilde{\boldsymbol{\Phi}}_k(Z) \\ \partial_Z \tilde{\boldsymbol{\Phi}}_k(Z) \end{pmatrix}, \tag{35}$$

where $\tilde{\boldsymbol{\Phi}}_k(Z)$ stands as the generator of the solution space associated with the linear system (33).

3.3. Solution for 2D-vector homogeneous wave equation

The solution of the two-waves equations (20) associated with the initial boundary conditions (21) are searched under decomposition

$$\boldsymbol{\mathcal{Y}}(Z,\tau) = \boldsymbol{\mathcal{Y}}_h(Z,\tau) + \boldsymbol{\mathcal{Y}}_p(Z,\tau), \tag{36}$$

where subscript h refers to homogeneous solution whilst subscript p refers to particular one associated with non-homogeneous boundary conditions. The latter is regarded as a separated variable time-space function. The Z behavior is furthermore decomposed into the first order polynomial

$$\boldsymbol{\mathcal{Y}}_p(Z,\tau) = Z\boldsymbol{\mathcal{Y}}_p^1(\tau) + \boldsymbol{\mathcal{Y}}_p^0(\tau). \tag{37}$$

Since the previous expression should ensures the boundary condition system spelled out in (22), it consequently results

$$\begin{pmatrix} \boldsymbol{\mathcal{N}} & \boldsymbol{\mathcal{M}} \\ \boldsymbol{\mathcal{Q}} & \boldsymbol{\mathcal{Q}} + \boldsymbol{\mathcal{R}} \end{pmatrix}_{(8\times 8)} \begin{pmatrix} \boldsymbol{\mathcal{Y}}_p^0(\tau) \\ \boldsymbol{\mathcal{Y}}_p^1(\tau) \end{pmatrix}_{(8\times 1)} = \boldsymbol{\mathcal{S}}_{(8\times 1)}(\tau). \tag{38}$$

The resolution of (38) then provides $\boldsymbol{\mathcal{Y}}_p$. The homogeneous component, $\boldsymbol{\mathcal{Y}}_h$, is hereby decomposed over the eigenvector base of the self-adjoint operator $\mathcal{H}$ so that

$$\boldsymbol{\mathcal{Y}} = \sum_{\mathcal{S}_p} a_k(\tau)\boldsymbol{\Phi}_k(Z) + \boldsymbol{\mathcal{Y}}_p(Z,\tau), \tag{39}$$

or, using $\tilde{\boldsymbol{\Phi}}_k(Z)$ in (35)

$$\boldsymbol{\mathcal{Y}}(Z,\tau) = \sum_{\mathcal{S}_p} \frac{a_k(\tau)\tilde{\boldsymbol{\Phi}}_k(Z)}{\|\tilde{\boldsymbol{\Phi}}_k(Z)\|} + \boldsymbol{\mathcal{Y}}_p(Z,\tau), \tag{40}$$

where $a_k(\tau)$ is the k^{th} mode time-dependent amplitude. Invoking the initial rest conditions (21), with definition of $\tilde{\mathbf{\Phi}}_k(Z)$ in (35), leads to,

$$a_k(0) = -\frac{\langle \boldsymbol{\mathcal{Y}}_p(Z,0), \tilde{\mathbf{\Phi}}_k(Z)\rangle}{\|\tilde{\mathbf{\Phi}}_k(Z)\|} \text{ , and, } \partial_\tau a_k(0) = -\frac{\langle \partial_\tau \boldsymbol{\mathcal{Y}}_p(Z,0), \tilde{\mathbf{\Phi}}_k(Z)\rangle}{\|\tilde{\mathbf{\Phi}}_k(Z)\|}. \quad (41)$$

The proposed decomposition of $\boldsymbol{\mathcal{Y}}(Z,\tau)$ in (40) must hereby satisfy the wave equation system (20). Regarding the definition of $\mathcal{H}$ in (23) with the spatial polynomial decomposition of $\boldsymbol{\mathcal{Y}}_p$ in (37) it achieves as follows

$$\mathcal{H}\boldsymbol{\mathcal{Y}}_p = \mathbf{0}, \quad (42)$$

so that

$$\left(\partial_\tau^2 - \mathcal{H}\right) \sum_{\mathcal{S}_\mathcal{P}} \frac{a_k(\tau)\tilde{\mathbf{\Phi}}_k(Z)}{\|\tilde{\mathbf{\Phi}}_k(Z)\|} = -\partial_\tau^2 \boldsymbol{\mathcal{Y}}_p. \quad (43)$$

Now projecting over $\tilde{\mathbf{\Phi}}_k(Z)$ leads to,

$$\left(\partial_\tau^2 + \lambda_k^2\right) a_k(\tau) = -\partial_\tau^2 \frac{\langle \boldsymbol{\mathcal{Y}}_p, \tilde{\mathbf{\Phi}}_k(Z)\rangle}{\|\tilde{\mathbf{\Phi}}_k(Z)\|}. \quad (44)$$

This ordinary differential equation, having initial conditions (41), is solved leading to (Further details provided in Appendix C)

$$a_k(\tau) = \lambda_k \int_0^\tau \frac{\langle \boldsymbol{\mathcal{Y}}_p, \tilde{\mathbf{\Phi}}_k(Z)\rangle(t)}{\|\tilde{\mathbf{\Phi}}_k(Z)\|} \sin\left(\lambda_k(\tau - t)\right) dt - \frac{\langle \boldsymbol{\mathcal{Y}}_p, \tilde{\mathbf{\Phi}}_k(Z)\rangle}{\|\tilde{\mathbf{\Phi}}_k(Z)\|}. \quad (45)$$

Finally, combining the (45) with the $\boldsymbol{\mathcal{Y}}$'s definition in (40) results in

$$\boldsymbol{\mathcal{Y}}(Z,\tau) = \sum_{\mathcal{S}_\mathcal{P}} \lambda_k \left(\int_0^\tau \frac{\langle \boldsymbol{\mathcal{Y}}_p, \tilde{\mathbf{\Phi}}_k(Z)\rangle(t)}{\|\tilde{\mathbf{\Phi}}_k(Z)\|^2} \sin\left(\lambda_k(\tau - t)\right) dt \right) \tilde{\mathbf{\Phi}}_k(Z) - \sum_{\mathcal{S}_\mathcal{P}} \frac{\langle \boldsymbol{\mathcal{Y}}_p, \tilde{\mathbf{\Phi}}_k(Z)\rangle}{\|\tilde{\mathbf{\Phi}}_k(Z)\|^2} \tilde{\mathbf{\Phi}}_k(Z) + \boldsymbol{\mathcal{Y}}_p(Z,\tau). \quad (46)$$

In the following, (46) is used to cross-check/validate predictions of two well-known configurations of liquid filled pipes problem: (i) a constant pressure tank with a fixed instantaneous closing valve (Cf Fig. 1a), (ii) a constant pressure tank with a free instantaneous closing valve (Cf Fig. 1b). The related upstream and downstream boundary conditions are analyzed in depth

in [32]. It is important to mention that, in the special case of boundary conditions having no pressure/velocity coupling, the previous general framework associated with four coupled waves equations boils down into two decoupled two-waves propagation, not only sharing the same spectrum, but also the same modes and amplitudes. In other words, in the absence of coupling between pressure and velocity in the boundary conditions, the four-waves equations set degenerates into a two-waves one. In the next section, we consider this simplified degenerate case for two classes of boundary conditions.

4. Application to specific boundary conditions

4.1. Constant pressure tank with a fixed instantaneous closing valve

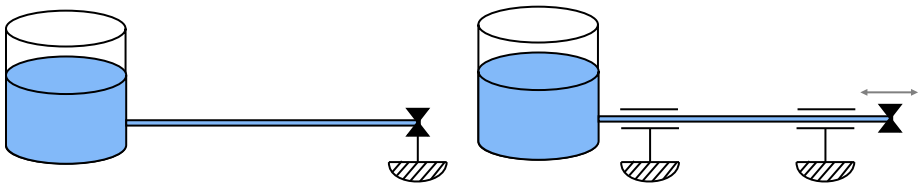

(a) First configuration : anchored valve (b) Second configuration : axially free valve

Figure 1: Boundary condition set investigated for the liquid filled pipe problem

Fluid (water)	Solid (steel)
$\rho_f = 1000\ kg \cdot m^3$	$\rho_s = 7900\ kg \cdot m^{-3}$
$\mathcal{K} = 2.1\ GPa$	$E = 210\ GPa$
$\nu_f = 9.493 \cdot 10^{-7}\ m^2 s^{-1}$	$\nu_s = 0.3$
	$R_0 = 0.395\ m$
	$e = 0.008\ m$
	$L = 20\ m$

Table 1: Physical and geometrical properties for the analysis of the reservoir-pipe-valve system (anchored and free). The parameter values are extracted from [27].

All comparisons and analysis are based upon the parameter set introduced in Table 1. The natural fluid-pulse frequency of both configurations is found equal to $f_0 \approx 8Hz$, whereas the cutoff frequency is $f_{Kc} \approx 2060Hz$. The λ_k should then lie in the range $\lambda_k \in [-247.6, 247.6]$ in order to fulfill the modeling assumptions (Cf. section 2.1).

4.1.1. Analytical solution

In the first configuration (Cf. Figure 1a), the pipe is supposed perfectly anchored, both upstream and downstream. Thus, no solid axial movement occurs at both pipe dead-ends which can be modeled as a Dirichlet-Dirichlet condition on the axial solid displacement acceleration. Furthermore, the reservoir does not impede any upstream pressure fluctuation which can be interpreted as an homogeneous Dirichlet condition for the pressure. Finally, an instantaneous valve closure downstream is modeled by a Dirac distribution, $\delta(\tau)$ (i.e. singular perturbation), acting on the axial fluid acceleration. The four boundary condition thereby achieves as follows

$$P(0,\tau) = 0 \quad , \partial_\tau W(1,\tau) = -\delta(\tau), \quad \partial_\tau \dot{\zeta}(0,\tau) = \partial_\tau \dot{\zeta}(1,\tau) = 0, \tag{47}$$

or otherwise regarding (4)&(6)

$$P(0,\tau) = 0 \quad , \partial_Z P(1,\tau) = \delta(\tau), \quad \partial_Z \sigma(0,\tau) = \partial_Z \sigma(1,\tau) = 0. \tag{48}$$

The initial Dirichlet conditions upon both fluid and solid acceleration quantities thus turn into Neumann conditions for the fluid pressure and solid stress fields. Invoking base-change (17)-(19), whilst introducing

$$\beta = \frac{c_+}{c_-}\frac{c_-^2 - 1}{c_+^2 - 1}, \tag{49}$$

the matrices introduced in (22) describing boundary conditions in the diagonalized basis can be found explicitly

$$\boldsymbol{\mathcal{N}} = \begin{pmatrix} 1 & \frac{\beta c_-}{c_+} \\ 0 & 0 \end{pmatrix}, \quad \boldsymbol{\mathcal{M}} = \begin{pmatrix} 0 & 0 \\ 1 & 1 \end{pmatrix}, \quad \boldsymbol{\mathcal{Q}} = \mathbf{0}, \quad \boldsymbol{\mathcal{R}} = \boldsymbol{\mathcal{N}} + \boldsymbol{\mathcal{M}}, \tag{50}$$

and,

$$\boldsymbol{\mathcal{S}}(\tau) = \frac{\left(c_-^2 - 1\right)\delta(\tau)}{2\nu_s \mathcal{D}} \left(0, 0, 1, 0\right)^T, \tag{51}$$

The determination of the scalar-product weight parameter $\boldsymbol{\eta} \equiv (\eta_1, \eta_2)$, introduced in (27), is hereby overcame. Injecting boundary conditions (48) within self-adjointness one (27) for the couple of two 2D unknown column vectors

$$\left(\boldsymbol{\Psi}(Z), \boldsymbol{\Psi}'(Z)\right) = \left(\left(\psi_1(Z), \psi_2(Z)\right)^T, \left(\psi_1'(Z), \psi_2'(Z)\right)^T\right), \tag{52}$$

yields

$$\left[\partial_Z \Psi_1(0)\Psi_1^{'}(0) - \Psi_1(0)\partial_Z \Psi_1^{'}(0)\right]\left(\eta_1 + \eta_2 \frac{c_+^3}{\beta c_-^3}\right) = 0, \tag{53}$$

so that the relation between η_1 & η_2 can be found

$$\eta_2 = -\eta_1 \beta \left(\frac{c_-}{c_+}\right)^3. \tag{54}$$

Scalar product (25) then results in

$$\langle \mathbf{\Psi}, \mathbf{\Psi}^{'} \rangle = \eta_1 \int_0^1 \left[\Psi_1(z)\Psi_1^{'}(z) - \beta \left(\frac{c_-}{c_+}\right)^3 \Psi_2(z)\Psi_2^{'}(z)\right] dz. \tag{55}$$

The λ_k are hence solutions of the formal relation (34). Using $\boldsymbol{\mathcal{C}}_{\boldsymbol{\mathcal{P}}}^2$ in (19), boundary condition matrices (50) and $\mathbf{T}_s(Z)$ in (32), leads to the explicit (and simplified) transcendental equation

$$\beta \sin\left(\frac{\lambda_k}{c_-}\right)\cos\left(\frac{\lambda_k}{c_+}\right) - \sin\left(\frac{\lambda_k}{c_+}\right)\cos\left(\frac{\lambda_k}{c_-}\right) = 0. \tag{56}$$

The particular component of $\boldsymbol{\mathcal{P}}(Z,\tau)$, $\boldsymbol{\mathcal{P}}_p(Z,\tau)$, follows from the spatial polynomial decomposition (37) and the resolution of the linear system (38), whilst $\tilde{\mathbf{\Phi}}_k(Z)$ determination is found combining transfer matrix formulation (30), linear boundary condition system (33) and the associated boundary condition matrices (50)

$$\tilde{\mathbf{\Phi}}_k(Z) = \begin{pmatrix} \cos\left(\frac{\lambda_k}{c_-}Z\right) + \tan\left(\frac{\lambda_k}{c_-}\right)\sin\left(\frac{\lambda_k}{c_-}Z\right) \\ -\frac{c_+}{\beta c_-}\left[\cos\left(\frac{\lambda_k}{c_+}Z\right) + \tan\left(\frac{\lambda_k}{c_+}\right)\sin\left(\frac{\lambda_k}{c_+}Z\right)\right] \end{pmatrix}, \tag{57}$$

$$\boldsymbol{\mathcal{P}}_p(Z,\tau) = \frac{\delta(\tau)Z}{\det\left(\mathbf{\Pi_P}\right)}\begin{pmatrix} 1 \\ -1 \end{pmatrix}. \tag{58}$$

Further details on the derivation are provided in Appendix D. The combination of $\tilde{\mathbf{\Phi}}_k(Z)$ and $\boldsymbol{\mathcal{P}}_p(Z,\tau)$ vectors in (57)-(58) fulfill the expression $\boldsymbol{\mathcal{P}}(Z,\tau)$ in (46)

$$\boldsymbol{\mathcal{P}}(Z,\tau) - \boldsymbol{\mathcal{P}}_p(Z,\tau) = \sum_{\mathcal{S}_{\mathcal{P}}} \frac{\langle Z\begin{pmatrix} 1 \\ -1 \end{pmatrix}, \tilde{\mathbf{\Phi}}_k(Z)\rangle}{\det\left(\mathbf{\Pi_P}\right)\|\tilde{\mathbf{\Phi}}_k(Z)\|^2}\tilde{\mathbf{\Phi}}_k(Z)\left[\lambda_k \sin\left(\lambda_k \tau\right) - \delta(\tau)\right], \tag{59}$$

with,

$$\|\tilde{\mathbf{\Phi}}_k(Z)\|^2 = \frac{c_+\beta\cos^2\left(\frac{\lambda_k}{c_+}\right) - c_-\cos^2\left(\frac{\lambda_k}{c_-}\right)}{2c_+\beta\cos^2\left(\frac{\lambda_k}{c_+}\right)\cos^2\left(\frac{\lambda_k}{c_-}\right)}, \tag{60}$$

$$\langle Z\begin{pmatrix}1\\-1\end{pmatrix}, \tilde{\mathbf{\Phi}}_k(Z)\rangle = \frac{c_-^2\left(\cos\left(\frac{\lambda_k}{c_+}\right) - \cos\left(\frac{\lambda_k}{c_-}\right)\right)}{\lambda_k^2\cos\left(\frac{\lambda_k}{c_-}\right)\cos\left(\frac{\lambda_k}{c_+}\right)}. \tag{61}$$

4.1.2. ν_s parametric analysis

Since the Poisson coupling, relies on the Poisson modulus, it is relevant to investigate the ν_s dependency of the previous analytical expressions. By performing an asymptotic analysis, without considering FSI effects, [31, 43] found the spectrum associated with the pressure waves in the fluid. It is interesting to point out that the solution (59) converges toward the [31]'s leading-order one, as $\nu_s \to 0$. The [31]'s leading-order solution is

$$\lambda_k = \pi\left(1+\frac{k}{2}\right), \quad \forall k \in \mathbb{N}, \tag{62}$$

$$P(Z,\tau) = 2\sum_{k=0}^{\infty}(-1)^k\frac{\sin\left(\lambda_k Z\right)\sin\left(\lambda_k\tau\right)}{\lambda_k}. \tag{63}$$

A more detailed derivation of this result is provided in Appendix E. The ν_s dependence of both spectrum and pressure waves compared with no-FSI solutions (i.e $\nu_s = 0$ case) is further illustrated in Figure 2. Figure 2b shows that the spectrum of the first configuration can be interpreted as the union between the fluid vibration modes (continuous blue lines) and the pure elastic ones (red squared lines). The solid and fluid contributions to the spectrum are easily identified from the analysis of the no-(FSI) configuration, as theoretically detailed in Appendix E (Cf. (E.10)). In Figure 2a the (59) solution for $\nu_s = 0$ is confronted with the [31]'s leading order one and, for comparison with the $\nu_s = 0.3$ case, all other parameters being equals. One can observed that high-frequency pressure oscillations progressively growing in time are revealed by the FSI coupling. These high-frequency oscillations are nevertheless expected to be damped by the viscous fluid friction or some structural energetic losses. In the $\nu_s \to 0$ limit, [31]'s pointed-out that fluid viscous friction exponentially damps each resonant mode. This feature remains when

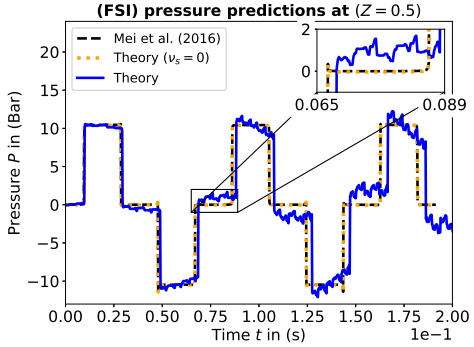

(a) Pressure response at $Z = 0.5$

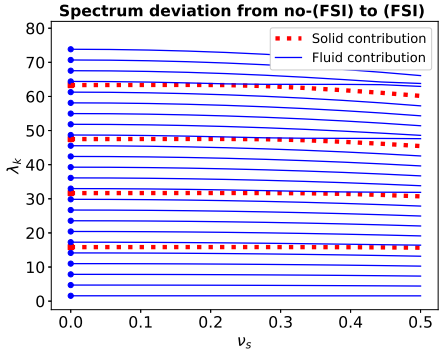

(b) Spectrum (28 first eigenvalues) versus the Poisson modulus ν_s in the Korteweg's frequency range.

Figure 2: Impact of the (FSI) on the expected: (a) pressure response and, (b) spectrum for the first case configuration (Cf. Fig. 1a). In (a), the [31]'s leading order solution is provided, in black dashed lines, as to point out the convergence of the models. In (b), as ν_s vary, some eigenvalues come close one-another, but a careful inspection shows no cross-over between the depicted eigenvalues.

considering (FSI) interactions, as analyzed in [41]. When dealing with time-scale of the order of the advective pulse wave speed one, i.e. $O\left(L/c_p\right)$, the energetic losses are shown [6, 31] to have a negligible impact on the overall coupled dynamic.

4.2. Constant pressure tank with free instantaneous closing valve

A second configuration, depicted in Figure 1b, is hereby analyzed whereby the downstream valve is free to move axially. Hence, upstream, the same conditions as in (48) are applied, with homogeneous Neumann condition for the axial stress and homogeneous Dirichlet condition for the pressure field set as

$$P(0,\tau) = 0 \quad \text{, and,} \quad \partial_Z \sigma(0,\tau) = 0. \tag{64}$$

Downstream, the boundary condition strongly differs from the previous configuration from valve longitudinal motion. Since $\alpha(2+\alpha)$ is equal to the ratio of solid surface (i.e. $\pi e R_0\left(2+\alpha\right)$) to the fluid one (i.e. πR_0^2), the static equilibrium of forces at valve location, in the absence of valve's inertia, reduces to

$$\alpha(2+\alpha)\sigma(1,\tau) = P(1,\tau). \tag{65}$$

The axial solid and fluid acceleration matching at the valve further imposes

$$\partial_\tau W(1,\tau) - \alpha \partial_\tau \dot{\zeta}(1,\tau) = -\delta(\tau), \tag{66}$$

or otherwise regarding relations (4) & (6)

$$\partial_Z P(1,\tau) + \mathcal{D}\partial_Z \sigma(1,\tau) = \delta(\tau). \tag{67}$$

The α constant in (66) arises from dimensionless arguments and can be obtained regarding the Appendix B. As the valve is now free to move, the downstream boundary condition slightly differs form the one provided in (47). Indeed, the acceleration perturbation is now applied to the relative acceleration of the fluid with respect to the tube motion, [32]. Considering change-basis (17)-(18) and introducing parameters

$$\kappa_\pm = \mathcal{D} + \frac{2\nu_s \mathcal{D}}{c_\pm^2 - 1} \quad \text{, and,} \quad \frac{\beta c_- \kappa_-}{c_+ \kappa_+} = \frac{1 - \frac{2\nu_s \mathcal{D}}{\alpha(2+\alpha)(c_+^2-1)}}{1 - \frac{2\nu_s \mathcal{D}}{\alpha(2+\alpha)(c_-^2-1)}}, \tag{68}$$

yields

$$\boldsymbol{\mathcal{N}} = \begin{pmatrix} 1 & \frac{\beta c_-}{c_+} \\ 0 & 0 \end{pmatrix}, \quad \boldsymbol{\mathcal{M}} = \begin{pmatrix} 0 & 0 \\ 1 & 1 \end{pmatrix}, \quad \boldsymbol{\mathcal{Q}} = \begin{pmatrix} 0 & 0 \\ 1 & \frac{\beta c_- \kappa_-}{c_+ \kappa_+} \end{pmatrix}, \quad \boldsymbol{\mathcal{R}} = \begin{pmatrix} \kappa_- & \kappa_+ \\ 0 & 0 \end{pmatrix}, \tag{69}$$

with the forcing term

$$\boldsymbol{\mathcal{S}}(\tau) = \delta(\tau)\,(0,0,1,0)^T \tag{70}$$

The non-trivial parametric relation (68) is established in Appendix F. The same footsteps are hereby applied to overcome the resolution of $\boldsymbol{\mathcal{P}}(Z,\tau)$. The self-adjoint condition (27) leads to

$$\left(\eta_1 + \left(\frac{c_+}{c_-}\right)^3 \frac{\eta_2}{\beta}\right) \left[\partial_Z \Psi_1(Z)\Psi_1'(Z) - \Psi_1(Z)\partial_Z \Psi_1'(Z)\right]_0^1 = 0, \tag{71}$$

so that

$$\eta_2 = -\eta_1 \beta \left(\frac{c_-}{c_+}\right)^3. \tag{72}$$

Thereby, scalar product defined in (25) remains identical to (55). A combination boundary condition matrices (69), the spectrum condition (34) and

transfer matrices (31)-(32) expressions, leads to the following (simplified) transcendental equation

$$\left(1+\left(\frac{\kappa_-}{\kappa_+}\right)^2\right)\cos\left(\frac{\lambda_k}{c_+}\right)\cos\left(\frac{\lambda_k}{c_-}\right) + \frac{1}{\beta}\left(1+\left(\frac{\beta\kappa_-}{\kappa_+}\right)^2\right)\sin\left(\frac{\lambda_k}{c_+}\right)\sin\left(\frac{\lambda_k}{c_-}\right) = \frac{2\kappa_-}{\kappa_+}. \quad (73)$$

Finally, one can find $\tilde{\mathbf{\Phi}}_k(Z)$ and $\boldsymbol{\mathcal{P}}_p(Z,\tau)$ vectors fields using boundary condition system (22) and boundary condition matrices (69), leading to (detailed derivation provided in Appendix G),

$$\tilde{\mathbf{\Phi}}_k(Z) = \begin{pmatrix} \cos\left(\frac{\lambda_k}{c_-}Z\right)+\xi_k\sin\left(\frac{\lambda_k}{c_-}Z\right) \\ -\frac{c_+}{\beta c_-}\left[\cos\left(\frac{\lambda_k}{c_+}Z\right)+\beta\xi_k\sin\left(\frac{\lambda_k}{c_+}Z\right)\right]\end{pmatrix}, \quad (74)$$

$$\boldsymbol{\mathcal{P}}_p(Z,\tau) = \frac{\delta(\tau)}{\kappa_--\kappa_+}\left[\begin{pmatrix}1\\-1\end{pmatrix}Z-\gamma\begin{pmatrix}1\\-\frac{c_+}{\beta c_-}\end{pmatrix}\right], \quad (75)$$

with,

$$\xi_k=\frac{\sin\left(\frac{\lambda_k}{c_-}\right)-\frac{\kappa_+}{\beta\kappa_-}\sin\left(\frac{\lambda_k}{c_+}\right)}{\cos\left(\frac{\lambda_k}{c_-}\right)-\frac{\kappa_+}{\kappa_-}\cos\left(\frac{\lambda_k}{c_+}\right)} \text{ , and, } \gamma=\frac{\kappa_-c_-\beta-c_+\kappa_+}{c_+\left(\kappa_--\kappa_+\right)}. \quad (76)$$

Since, according to the scalar product (55) and (72)

$$\|\tilde{\mathbf{\Phi}}_k(Z)\|^2 = -\frac{c_-+c_-\beta^2\xi_k^2-c_+\beta\left(\xi_k^2+1\right)}{2c_+\beta}+c_-\xi_k\frac{\cos^2\left(\frac{\lambda_k}{c_+}\right)-\cos^2\left(\frac{\lambda_k}{c_-}\right)}{\lambda_k} + c_-\frac{\frac{\beta^2\xi_k^2-1}{\beta}\sin\left(\frac{2\lambda_k}{c_+}\right)-\left(\xi_k^2-1\right)\sin\left(\frac{2\lambda_k}{c_-}\right)}{4\lambda_k}, \quad (77)$$

and

$$\langle\boldsymbol{\mathcal{P}}_p(Z,\tau),\tilde{\mathbf{\Phi}}_k(Z)\rangle = \frac{c_-\delta(\tau)}{\kappa_--\kappa_+}\left(\mathcal{F}_--\frac{c_-\mathcal{F}_+}{c_+}-\gamma\left[\mathcal{G}_+-\mathcal{G}_-\right]\right) \quad (78)$$

$$\mathcal{F}_\pm = \frac{\cos\left(\frac{\lambda_k}{c_\pm}\right)\left[c_\pm-\theta_\pm\lambda_k\xi_k\right]+\sin\left(\frac{\lambda_k}{c_\pm}\right)\left[\lambda_k+c_\pm\theta_\pm\xi_k\right]-c_\pm}{\lambda_k^2}, \quad (79)$$

$$\mathcal{G}_\pm = \frac{\theta_\pm\xi_k\left(\cos\left(\frac{\lambda_k}{c_\pm}\right)-1\right)-\sin\left(\frac{\lambda_k}{c_\pm}\right)}{\theta_\pm\lambda_k}, \quad (80)$$

$$\theta_- = 1, \quad \theta_+=\beta, \quad (81)$$

the expression of $\boldsymbol{\mathcal{P}}(Z,\tau)$ in (46) pursues

$$\boldsymbol{\mathcal{P}}(Z,\tau) - \boldsymbol{\mathcal{P}}_p(Z,\tau) = \\ c_- \sum_{\mathcal{S}_{\mathcal{P}}} \frac{\mathcal{F}_- - \frac{c_-\mathcal{F}_+}{c_+} - \gamma\left[\mathcal{G}_+ - \mathcal{G}_-\right]}{(\kappa_- - \kappa_+)\left\|\tilde{\boldsymbol{\Phi}}_k(Z)\right\|^2} \tilde{\boldsymbol{\Phi}}_k(Z)\left[\lambda_k \sin\left(\lambda_k\tau\right) - \delta(\tau)\right]. \quad (82)$$

The above expressions (77)-(81) have been cross-checked using formal calculus softwares.

4.3. Comparisons and illustrations

We now discuss quantitative illustrations of the provided analytical solutions so as to demonstrate their matching with previously published numerical results. Since many previous contributions have considered Fourier representation of test cases, our theoretical predictions for the discrete spectrum associated with discrete frequency peaks are first analyzed. The spectrum formally given by general relation (34) and more specifically by explicit simple transcendent relations (56) and (73) are compared to the Fourier transform peaks in Figure 3. The determinant's zeros, λ_k, are classically related to the natural frequencies accordingly to the following linear law, [28]

$$f_k = \lambda_k f_0, \quad (83)$$

where f_k is the k^{th} natural frequency expressed in Hz and f_0 is the natural acoustic fluid frequency introduced in (8). A perfect matching of the predicted peaks (dotted lines) with the numerical one can be observed in Figure 3 . More precisely, Figure 3a compares [44]'s results with our prediction for boundary conditions (i) (Cf Fig. 1a) whereas Figure 3b consider [28]'s prediction for boundary conditions (ii) (Cf Fig. 1b). These theoretical predictions are matched to numerical results without any adjusted parameters. More quantitative comparison between the numerical peaks and their theoretical predictions are provided in table 2 with excellent agreement.
Temporal predictions are also compared with MOC numerical results so as to test every details of the analytical solutions, i.e. not only the spectrum but also the eigenmodes and their amplitudes. Figure 4 provides this comparison with [27]'s MOC solutions for the set of parameters presented in Table 1. In each case a nearly perfect matching between the theoretical prediction and the numerical computation can be observed. Zoom are provided for high-frequency fidelity check. The resulting mismatch might be attributable to

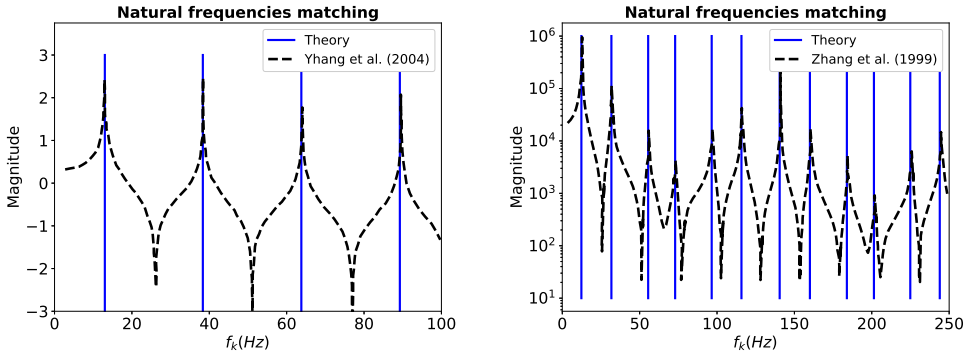

(a) First configuration (Cf Fig. 1a)

(b) Second configuration (Cf Fig. 1b).

Figure 3: Continuous black-lines : Fourier transform of the pressure field at valve location within the pipe versus frequency f. Blue dotted lines : spectrum eigenvalues. (a) Comparison between [44]'s prediction at the valve location with eigenvalues obtained from transcendental equation (56). (b) comparison between [28]'s pressure prediction at the valve location with prediction from transcendental equation (73).

First boundary condition (i) (Cf Fig. 1a)			Second boundary condition (ii) (Cf Fig. 1b)		
[44] (Hz)	Theorical (Hz)	Δ (%)	[28] (Hz)	Theorical (Hz)	Δ (%)
13.1	13.00	0.8	12	12.4	3.2
38.5	38.3	0.5	32	31.8	0.6
64.0	63.8	0.3	56	55.5	0.9
89.6	89.3	0.3	73	72.9	0.1
115.1	114.6	0.4	97	96.6	0.4
131.8	131.7	0.08	116	115.8	0.2
141.3	140.8	0.3	141	140.5	0.4
166.6	165.9	0.4	161	160.0	0.6
192.1	191.4	0.4	185	183.9	0.6
			202	201.4	0.3
			226	224.9	0.5
			245	243.9	0.5

Table 2: Comparative analysis of natural frequencies for the two study configurations. For each encountered frequency, the relative error $\Delta(\%)$ is estimated.

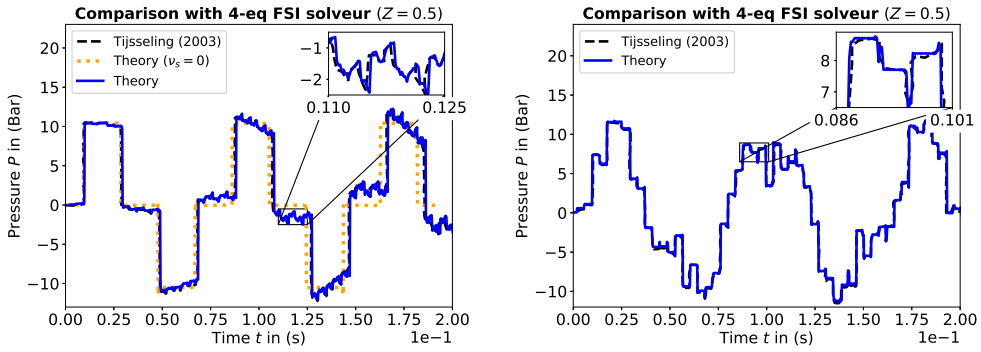

(a) First configuration (Cf Fig. 1a)

(b) Second configuration (Cf Fig. 1b).

Figure 4: Comparison between pressure field analytical solution at middle pipe location (continuous blue lines) with MOC solutions (dotted black lines). Non-FSI solutions (i.e $\nu_s = 0$) are provided for illustration in brown dotted lines. Insets provide a zoom for careful check.

the inaccuracy of data collection from [27]. No parameter adjustment have been used.

5. Sensitivity matrix evaluation

5.1. Wave speed, $c_\pm$, deviations

From the analytical expressions of $c_\pm$ in (15), the respective derivation of the dimensionless wave speeds are deduced upon dimensionless variables describing the fluid structure interactions. The parametric dependence of $c_\pm\left(\frac{E}{K}, \nu_s, \mathcal{D}, \alpha\right)$ is known so that any derivative $\frac{\partial c_\pm}{\partial X}$ (X being any structural parameter embedded in parameters $\frac{E}{K}$, ν_s, $\mathcal{D}$ in (3) and α) in (1) is possible to compute analytically. In order to simplify the algebraic expressions the

squared wave speeds (15) derivatives are evaluated

$$\frac{\partial c_{\pm}^2}{\partial \alpha} = \mu_c \frac{1+\alpha}{\alpha\,(2+\alpha)} \left[1 + \pm \frac{2\nu_s^2 - 1 + 2\nu_s \mathcal{D} + \mu_a}{\sqrt{\left(c_+^2 + c_-^2\right)^2 - 4\mathcal{C}_s^2}} \right], \tag{84}$$

$$\frac{\partial c_{\pm}^2}{\partial \left(\frac{E}{K}\right)} = \frac{\mathcal{D}}{2} \left[1 \pm \frac{\mu_a + 2\nu_s \mathcal{D} - 1}{\sqrt{\left(c_+^2 + c_-^2\right)^2 - 4\mathcal{C}_s^2}} \right] \tag{85}$$

$$\frac{\partial c_{\pm}^2}{\partial \nu_s} = \frac{1}{2} \left[2\mathcal{D} \pm \frac{4\nu_s \left(\mathcal{D}^2 - \mu_c\right) + 4\mathcal{D}\left(\frac{\mu_a - 1}{2} - 1\right)}{\sqrt{\left(c_+^2 + c_-^2\right)^2 - 4\mathcal{C}_s^2}} \right], \tag{86}$$

$$\frac{\partial c_{\pm}^2}{\partial \left(\frac{E}{K}\right)} = \frac{\mathcal{D}}{2} \left[1 \pm \frac{\mu_a + 2\nu_s \mathcal{D} - 1}{\sqrt{\left(c_+^2 + c_-^2\right)^2 - 4\mathcal{C}_s^2}} \right], \tag{87}$$

$$\frac{\partial c_{\pm}^2}{\partial \mathcal{D}} = \frac{1}{2\mathcal{D}} \left[\mu_a + 2\nu_s \mathcal{D} \pm \frac{\left(1 + \mu_a + 2\nu_s D\right)\left(\mu_a + 2\nu_s \mathcal{D}\right) - 2\mathcal{C}_s^2}{\sqrt{\left(c_+^2 + c_-^2\right)^2 - 4\mathcal{C}_s^2}} \right], \tag{88}$$

where $\mu_a = \mathcal{D}\left(2 + \frac{E}{K} + \frac{4}{\alpha(2+\alpha)}\right)$ and, $\mu_c = -\frac{4\mathcal{D}}{\alpha(2+\alpha)}$ are defined in (E.2)-(E.4). From (84)-(88) the velocity derivatives can easily be deduced from

$$\partial_X c_{\pm} = \frac{1}{2c_{\pm}} \partial_X c_{\pm}^2. \tag{89}$$

5.2. Sensitivity matrix for boundary condition (i)

From (56) it is possible to find an analytical expression of the sensitivity of the eigenvalues λ_k with respect to the parameters set $(\nu_s\alpha, E/K, \mathcal{D})$. Using (49) one gets

$$\frac{\partial \beta}{\partial X} = \frac{\partial \beta}{\partial c_-}\frac{\partial c_-}{\partial X} + \frac{\partial \beta}{\partial c_+}\frac{\partial c_+}{\partial X}, \tag{90}$$

$$\frac{\partial \beta}{\partial c_{\pm}} = \mp \frac{\beta}{c_{\pm}} \frac{c_{\pm}^2 + 1}{c_{\pm}^2 - 1}, \tag{91}$$

whilst from (56) one gets

$$\frac{\partial \lambda_k}{\partial X} = \frac{-c_-\,\partial_X \beta \tan\left(\frac{\lambda_k}{c_-}\right) + \frac{\lambda_k}{c_-}\left(\beta \partial_X c_- - \left(\frac{c_-}{c_+}\right)^2 \partial_X c_+ + \tan\left(\frac{\lambda_k}{c_-}\right)\tan\left(\frac{\lambda_k}{c_+}\right)\left[\partial_X c_- - \beta\left(\frac{c_-}{c_+}\right)^2 \partial_X c_+\right]\right)}{\beta - \frac{c_-}{c_+} + \tan\left(\frac{\lambda_k}{c_-}\right)\tan\left(\frac{\lambda_k}{c_+}\right)\left[1 - \beta\frac{c_-}{c_+}\right]}. \tag{92}$$

The spectrum sensitivity of the first configuration (Cf. Fig. 1a) is depicted in Figures 5a-5d, for the first five eigenmodes. The sensitivity analysis of

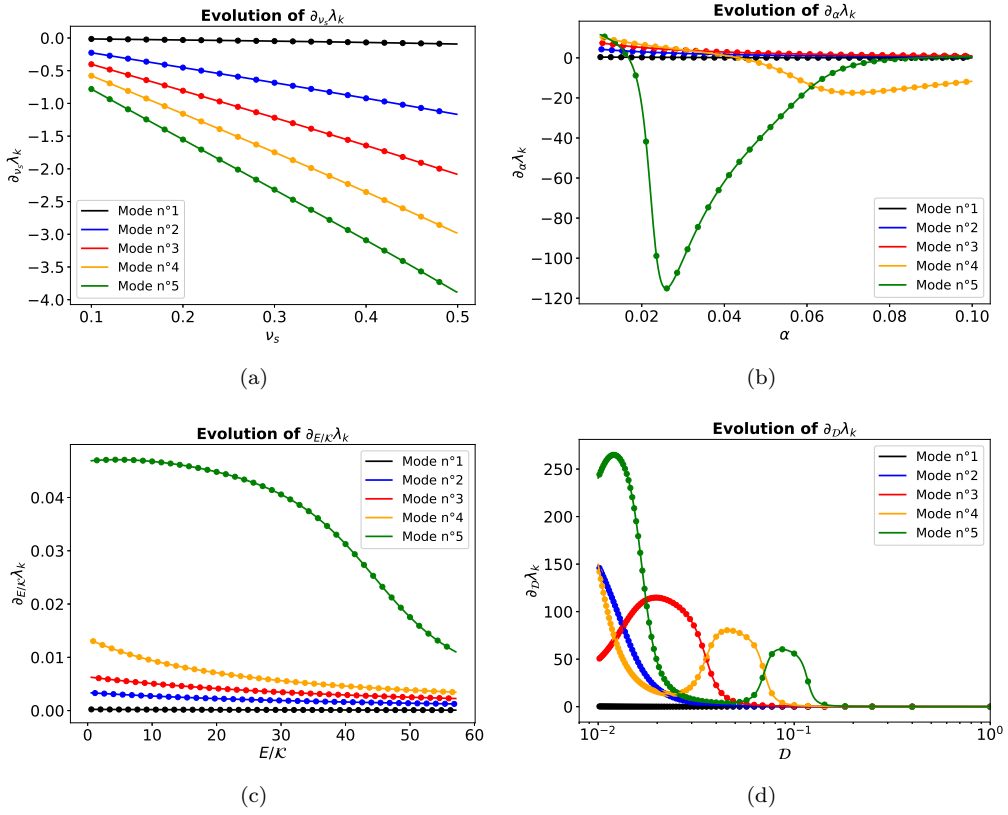

Figure 5: Sensitivity analysis of the first five resonnant eigenmodes associated with the spectrum equation (56). (a) $\partial_{\nu_s}\lambda_k$. (b) $\partial_\alpha\lambda_k$. (c) $\partial_{(E/\mathcal{K})}\lambda_k$. (d) $\partial_{\mathcal{D}}\lambda_k$. The numerical gradients are depicted in continuous lines whereas the analytical expressions are represented by dotted lines.

the first configuration reveals an increased parametric dependence for higher modes. The higher the mode, the more sensitive it is to the dimensionless parameters variation. Furthermore, this analysis highlights a high sensitivity of the first five eigenmodes with respect to the density ratio $\mathcal{D}$ as depicted on Figure 5d, whilst the system is found weakly dependent on the E/K ratio, as illustrated in Figure 5c.

5.3. Sensitivity matrix for boundary condition (ii)

A similar footpath is hereby provided for the reservoir-pipe-free valve configuration. The spectrum transcendental equation derived in (73), which holds for the second configuration (Cf Fig. 1b), is found dependent upon a set of four dimensionless parameters namely $c_\pm$, β and

$$\kappa(c_\pm, \nu_s) = \frac{\kappa_-}{\kappa_+} \equiv \frac{c_+}{\beta c_-}\frac{c_-^2 - (1-2\nu_s)}{c_+^2 - (1-2\nu_s)}. \tag{93}$$

The derivative of κ with respect to the dimensionless quantity $X \equiv (\nu_s, \alpha, E/\mathcal{K}, \mathcal{D})$ thus achieves as follows

$$\partial_X \kappa = \frac{c_+}{c_-\beta}\left[\partial_X \kappa_r + \kappa_r\left(\frac{1}{c_+}\partial_X c_+ - \frac{1}{c_-}\partial_X c_- - \frac{1}{\beta}\partial_X \beta\right)\right] \tag{94}$$

$$\kappa_r = \frac{c_-^2 - (1-2\nu_s)}{c_+^2 - (1-2\nu_s)}, \tag{95}$$

$$\partial_X \kappa_r = \frac{2}{c_+^2 - (1-2\nu_s)}\left(c_- c_+\left(\frac{1}{c_+}\partial_X c_- - \frac{\kappa_r}{c_-}\partial_X c_+\right) + \partial_X \nu_s\,(1-\kappa_r)\right), \tag{96}$$

whereas from (73) one gets

$$\begin{aligned}
\partial_X \lambda_k = &-\frac{2\kappa\partial_X\kappa}{\tan\left(\frac{\lambda_k}{c_+}\right)\left[\frac{1+(\beta\kappa)^2}{\beta c_-} - \frac{1+\kappa^2}{c_+}\right] + \tan\left(\frac{\lambda_k}{c_-}\right)\left[\frac{1+(\beta\kappa)^2}{\beta c_+} - \frac{1+\kappa^2}{c_-}\right]} \\
&+ \frac{\tan\left(\frac{\lambda_k}{c_+}\right)\tan\left(\frac{\lambda_k}{c_-}\right)\left(\frac{1+(\beta\kappa)^2}{\beta^2}\partial_X\beta - 2\kappa\left[\beta\partial_X\kappa + \kappa\partial_X\beta\right]\right)}{\tan\left(\frac{\lambda_k}{c_+}\right)\left[\frac{1+(\beta\kappa)^2}{\beta c_-} - \frac{1+\kappa^2}{c_+}\right] + \tan\left(\frac{\lambda_k}{c_-}\right)\left[\frac{1+(\beta\kappa)^2}{\beta c_+} - \frac{1+\kappa^2}{c_-}\right]} \\
&+ 2\frac{\partial_X\kappa}{\cos\left(\frac{\lambda_k}{c_-}\right)\cos\left(\frac{\lambda_k}{c_+}\right)\left(\tan\left(\frac{\lambda_k}{c_+}\right)\left[\frac{1+(\beta\kappa)^2}{\beta c_-} - \frac{1+\kappa^2}{c_+}\right] + \tan\left(\frac{\lambda_k}{c_-}\right)\left[\frac{1+(\beta\kappa)^2}{\beta c_+} - \frac{1+\kappa^2}{c_-}\right]\right)} \\
&+\lambda_k\frac{\tan\left(\frac{\lambda_k}{c_+}\right)\left[\frac{1}{c_-}\partial_X c_-\frac{1+(\beta\kappa)^2}{\beta c_-} - \frac{1}{c_+}\partial_X c_+\frac{1+\kappa^2}{c_+}\right] + \tan\left(\frac{\lambda_k}{c_-}\right)\left[\frac{1}{c_+}\partial_X c_+\frac{1+(\beta\kappa)^2}{\beta c_+} - \frac{1}{c_-}\partial_X c_-\frac{1+\kappa^2}{c_-}\right]}{\tan\left(\frac{\lambda_k}{c_+}\right)\left[\frac{1+(\beta\kappa)^2}{\beta c_-} - \frac{1+\kappa^2}{c_+}\right] + \tan\left(\frac{\lambda_k}{c_-}\right)\left[\frac{1+(\beta\kappa)^2}{\beta c_+} - \frac{1+\kappa^2}{c_-}\right]}.
\end{aligned} \tag{97}$$

The derivative of the five first eigenmodes is once again investigated and their related variations with respect to $(\nu_s, \alpha, E/\mathcal{K}, \mathcal{D})$ are depicted in Figure 6a-6d. A very same sensitivity ordering is found for the second configuration. The density ratio variations remain the most sensitive parameter whereas the $\frac{E}{\mathcal{K}}$ ratio has little impact on the coupled dynamic. It is interesting to point-out that the higher eigenmodes are no longer the most sensitive in this second case, as illustrated in Figures 6a-6b. The boundary condition couplings, or junction couplings, occurring in the second configuration, then reshape the eigenmode structure and their sensitivity.

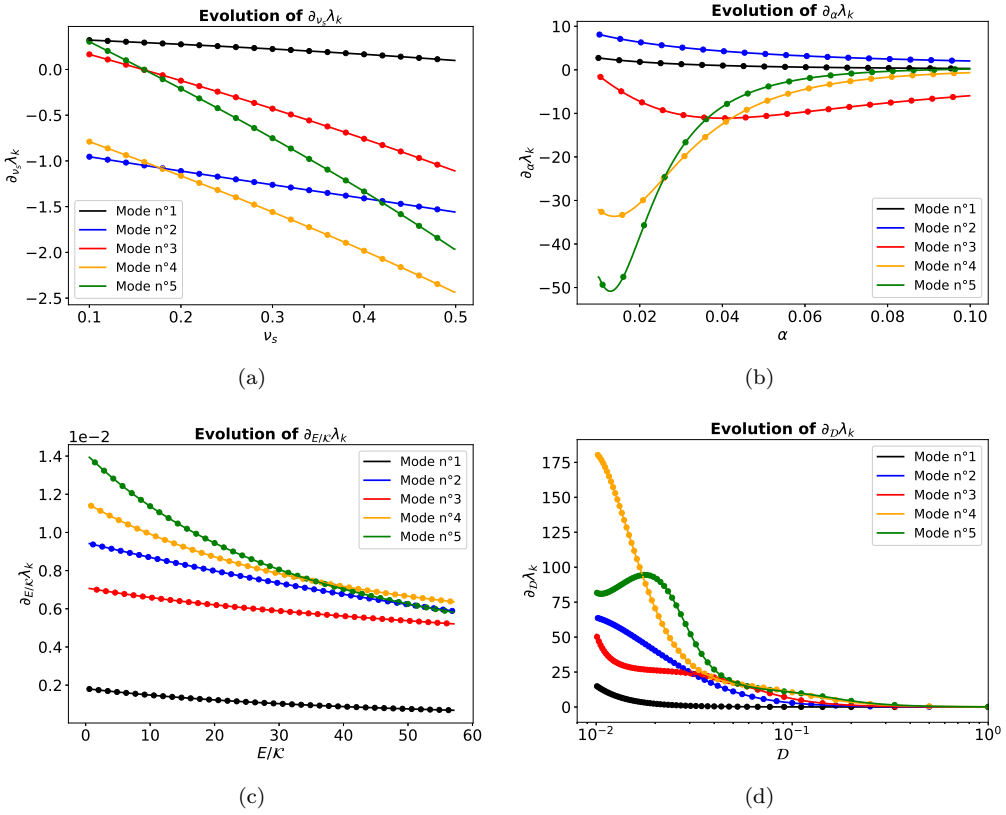

Figure 6: Same conventions as Figure 5 for spectrum equation (73). (a) $\partial_{\nu_s}\lambda_k$. (b) $\partial_\alpha\lambda_k$. (c) $\partial_{(E/\mathcal{K})}\lambda_k$. (d) $\partial_{\mathcal{D}}\lambda_k$.The numerical gradients are depicted in continuous lines whereas the analytical expressions are represented by dotted lines.

6. Conclusion

This contribution provide a theoretical framework for the analysis of analytical solutions for FSI pulsed waves propagation inside liquid filled tubes. This framework leads to an explicit spectrum derivation and analytical eigenmode decomposition. It favorably compares with previously published results. The spectrum sensitivity matrix has been computed explicitly with respect to (dimensionless) parameter derivatives, as well as wave velocity derivatives. The provided solutions might be used in various contexts associated with signal processing interpretation, parameter identification or boundary condition de-convolution inside liquid filled pipes.

Acknowledgement

This work was supported by the collaborative ANRT Grant CIFRE 2019/1453 co-funded by SETOM, dedicated society of Veolia for the public drinking water service of Toulouse Métropole operating under the brand Eau de Toulouse Métropole.
The authors have no competing interests to declare.

References

[1] N. Joukowsky, Uber den hydraulischen stoss in wasserleitungsro hren.(on the hydraulic hammer in water supply pipes) mé moires de l'académie impériale des sciences de st.-petersbourg., English translation, partly, by Simin 9 (1904).

[2] D. Korteweg, Ueber die fortpflanzungsgeschwindigkeit des schalles in elastischen rohren, on the speed of sound propagation in elastic tubes, Annalen der Physik 241 (12) (1878) 525–542.

[3] R. Skalak, An extension of the theory of waterhammer, Transactions of the ASME 78 (1956) 105–116.

[4] E. L. Holmboe, W. T. Rouleau, The Effect of Viscous Shear on Transients in Liquid Lines, J. Basic Eng. 89 (1) (1967) 174–180.

[5] W. Burmann, Water hammer in coaxial pipe systems, J. Hydraul. Eng. 101 (6) (1975) 699–715.

[6] D. D. Budny, D. C. Wiggert, F. J. Hatfield, The Influence of Structural Damping on Internal Pressure During a Transient Pipe Flow, J. Fluids Eng. 113 (3) (1991) 424–429.

[7] A. Tijsseling, Water hammer with fluid-structure interaction in thick-walled pipes, Computers & Structures 85 (2007) 844–851.

[8] A. S. Tijsseling, Fluid structure interaction in liquid filled pipe systems: a review, J Fluids Struct 10 (2) (1996) 109–146.

[9] S. Li, B. W. Karney, G. Liu, FSI research in pipeline systems – A review of the literature, J Fluids Struct 57 (2015) 277–297.

[10] D. Ferras, P. A. Manso, A. J. Schleiss, D. I. C. Covas, One-Dimensional Fluid–Structure Interaction Models in Pressurized Fluid-Filled Pipes: A Review, Applied Sciences 8 (10) (2018) 1844.

[11] S. Čanić, J. Tambača, G. Guidoboni, A. Mikelić, C. J. Hartley, D. Rosenstrauch, Modeling viscoelastic behavior of arterial walls and their interaction with pulsatile blood flow, SIAM J. Appl. Math. 67 (1) (2006) 164–193.

[12] T. J. Plona, B. K. Sinha, S. Kostek, S. Chang, Axisymmetric wave propagation in fluid-loaded cylindrical shells. II: Theory versus experiment, J. Acoust. Soc. Am. 92 (2) (1992) 1144–1155.

[13] B. K. Sinha, T. J. Plona, S. Kostek, S. Chang, Axisymmetric wave propagation in fluid-loaded cylindrical shells. i: Theory, J. Acoust. Soc. Am. 92 (2) (1992) 1132–1143.

[14] J. S. Walker, J. W. Phillips, Pulse Propagation in Fluid-Filled Tubes, Journal of Applied Mechanics 44 (1) (1977) 31–35.

[15] N. Kizilova, Pressure wave propagation in liquid-filled tubes of viscoelastic material, Fluid Dyn. 41 (2006) 434–446. doi:10.1007/s10697-006-0060-9.

[16] A. S. Tijsseling, C. S. W. Lavooij, Waterhammer with fluid-structure interaction, Applied Scientific Research 47 (3) (1990) 273–285.

[17] G. Liu, Y. Li, Vibration analysis of liquid-filled pipelines with elastic constraints, J. Sound Vib. 330 (13) (2011) 3166–3181.

[18] A. Keramat, M. Fathi-Moghadam, R. Zanganeh, M. Rahmanshahi, A. S. Tijsseling, E. Jabbari, Experimental investigation of transients-induced fluid–structure interaction in a pipeline with multiple-axial supports, J. Fluids Struct. 93 (2020) 102848. doi:10.1016/j.jfluidstructs.2019.102848.

[19] X. Wang, J. Lin, A. Keramat, M. S. Ghidaoui, S. Meniconi, B. Brunone, Matched-field processing for leak localization in a viscoelastic pipe: An experimental study, Mech Syst Signal Process 124 (2019) 459–478.

[20] X. Wang, D. Palomar, L. Zhao, M. Ghidaoui, R. Murch, Spectral-based methods for pipeline leakage localization, Journal of Hydraulic Engineering, ASCE 145 (3) (2019) 04018089.

[21] A. Keramat, B. Karney, M. S. Ghidaoui, X. Wang, Transient-based leak detection in the frequency domain considering fluid-structure interaction and viscoelasticity, Mech Syst Signal Process 153 (2021) 107500.

[22] A. Keramat, H. F. Duan, Spectral based pipeline leak detection using a single spatial measurement, Mech Syst Signal Process 161 (2021) 107940.

[23] T. C. Che, H. F. Duan, P. J. Lee, Transient wave-based methods for anomaly detection in fluid pipes: A review, Mech Syst Signal Process 160 (2021) 107874.

[24] H. F. Duan, P. J. Lee, Transient-based frequency domain method for dead-end side branch detection in reservoir pipeline-valve systems, J. Hydraul. Eng 142 (2) (2016) 04015042.

[25] H. F. Duan, Accuracy and sensitivity evaluation of tfr method for leak detection in multiple-pipeline water supply systems, Water Resour. Manage. 32 (2018) 2147–2164.

[26] M. W. Lesmez, D. C. Wiggert, F. J. Hatfield, Modal Analysis of Vibrations in Liquid-Filled Piping Systems, J. Fluid Eng. 112 (3) (1990) 311–318.

[27] A. S. Tijsseling, Exact solution of linear hyperbolic four-equation system in axial liquid-pipe vibration, J Fluids Struct 18 (2) (2003) 179–196.

[28] L. Zhang, A. Tijsseling, E. Vardy, FSI Analysis of Liquid-Filled Pipes, J. Sound Vib. 224 (1999) 69–99.

[29] Q. Li, K. Yang, L. Zhang, N. Zhang, Frequency domain analysis of fluid–structure interaction in liquid-filled pipe systems by transfer matrix method, INT J MECH SCI 44 (2002) 2067–2087.

[30] S. J. Li, G. M. Liu, W. t. Kong, Vibration analysis of pipes conveying fluid by transfer matrix method, Nuclear Engineering and Design 266 (2014) 78–88.

[31] C. C. Mei, H. Jing, Pressure and wall shear stress in blood hammer - Analytical theory, Mathematical Biosciences 280 (Oct. 2016).

[32] A. Tijsseling, Fluid-structure interaction in case of waterhammer with cavitation, Ph.D. thesis, Delft University of Technology (1993).

[33] M. H. Chaudhry, Applied Hydraulic Transients, 3rd Edition, Springer-Verlag, 2014.

[34] S. Li, B. W. Karney, G. Liu, FSI research in pipeline systems – a review of the literature, J. Fluids Struct. 57 (2015) 277–297. doi:10.1016/j.jfluidstructs.2015.06.020.

[35] T. C. Lin, G. W. Morgan, Wave Propagation through Fluid Contained in a Cylindrical, Elastic Shell, J. Acoust. Soc. Am. 28 (6) (1956) 1165–1176.

[36] F. Gaultier, J. Gilbert, J. Dalmont, R. Picó, Wave propagation in a fluid filled rubber tube: Theoretical and experimental results for korteweg's wave, Acta Acust. United Ac. 93 (2007) 333–344.

[37] M. S. Ghidaoui, M. Zhao, D. A. McInnis, D. H. Axworthy, A review of water hammer theory and practice, Appl. Mech. Rev. 58 (1) (2005) 49–76. doi:10.1115/1.1828050.

[38] A. Keramat, A. Tijsseling, Q. Hou, A. Ahmadi, Fluid–structure interaction with pipe-wall viscoelasticity during water hammer, J. Fluids Struct. 28 (2011) 434–455. doi:10.1016/j.jfluidstructs.2011.11.001.

[39] H. K. Aliabadi, A. Ahmadi, A. Keramat, Frequency response of water hammer with fluid-structure interaction in a viscoelastic pipe, Mech Syst Signal Process 144 (2020) 106848. doi:10.1016/j.ymssp.2020.106848.

[40] C. C. Mei, H. Jing, Effects of thin plaque on blood hammer—An asymptotic theory, Eur. J. Mech. B Fluids 69 (2018) 62–75. doi:10.1016/j.euromechflu.2018.01.004.

[41] A. Bayle, F. Plouraboué, Low Mach number theory of pressure waves inside an elastic tube, submitted (2022).

[42] M. Lewin, Eléments de théorie spectrale : le laplacien sur un ouvert borné, Master's thesis, CNRS & CEREMADE, Université Paris-Dauphine, PSL Research University (2017).

[43] G. D. C. Kuiken, Amplification of pressure fluctuations due to fluid-structure interaction, J Fluids Struct 2 (5) (1988) 425–435.

[44] K. Yang, Q. S. Li, L. Zhang, Longitudinal vibration analysis of multi-span liquid-filled pipelines with rigid constraints, J. Sound Vib. 273 (1) (2004) 125–147.

Appendix A. Nomenclature

Physics Constants		
ρ_f	Fluid density	$kg \cdot m^{-3}$
$\mathcal{K}$	Fluid bulk modulus	Pa
ρ_s	Solid density	$kg \cdot m^{-3}$
E	Young's modulus	Pa
ν_s	Poisson's modulus	
W_0	Order of magnitude of the steady velocity	$m \cdot s^{-1}$
Caracteristic velocities		
c_p	Modified Korteweg's wave speed / Fluid pulse wave speed	$m \cdot s^{-1}$
c_s	Solid elastic wave speed	$m \cdot s^{-1}$
$c_\pm$	Dimensionless coupled propagative modes wave speed	
Geometrical properties		
R_0	Inner initial tube's radius	m
e	Tube's thickness	m
L	Tubs's lenght	m
z	Dimensionall axial coordinate	m
Z	Dimensionless axil coordinate	
Dimensionless numbers		
ϵ	Ratio of the inner tube's radius by the tube's length	
α	Ratio of the tube's thickness by the inner tube's	
$\mathcal{C}_s$	Ratio of the solid elastic wave speed by the fluid pulse wave speed	
$\mathcal{D}$	Ratio of fluid density by the solid density	
Theorical elements		
$W(Z, \tau)$	Perturbed axial fluid velocity	

$P(Z,\tau)$	Perturbed fluid pressure
$\sigma(Z,\tau)$	Perturbed axial fluid stress tensor
$\dot{\zeta}(Z,\tau)$	Perturbed axial solid displacement velocity
$\mathcal{H}$	Self auto adjoint operator
$-\lambda_k^2$	Eigenvalue of $\mathcal{H}$
$a_k(\tau)$	Temporal amplitude of $\boldsymbol{\mathcal{Y}}_h$
f_k	Natural frequencies

Characteristic matrices

$\mathbf{Y}(Z,\tau)$	Perturbed dimensionless fluid and solid pressure-velocity vector
$\mathbf{P}(Z,\tau)$	Perturbed dimensionless pressure - stress vector
$\mathbf{C_P}$	Speed matrix of the pressure-stress wave equation
$\mathbf{C_W}$	Speed matrix of the velocity-displacement velocity wave equation
$\mathbf{C_Y}$	Speed matrix coupled fluid and solid pressure-velocity wave equation
$\boldsymbol{\mathcal{Y}}$	Perturbed dimensionless fluid and solid pressure-velocity vector within the diagonalisation basis
$\boldsymbol{\mathcal{Y}}_p(Z,\tau)$	Particular part of $\boldsymbol{\mathcal{Y}}$
$\boldsymbol{\mathcal{Y}}_h(Z,\tau)$	Homogeneous part of $\boldsymbol{\mathcal{Y}}$
$\boldsymbol{\mathcal{P}}$	Perturbed dimensionless pressure - stress vector within the diagonalisation basis
$\boldsymbol{\mathcal{P}}_h(Z,\tau)$	Homogeneous part of $\boldsymbol{\mathcal{P}}$
$\boldsymbol{\mathcal{P}}_p(Z,\tau)$	Particular part of $\boldsymbol{\mathcal{P}}$
$\boldsymbol{\mathcal{C}}_{\boldsymbol{\mathcal{P}}}$	Speed matrix within the diagonalisation basis
$\boldsymbol{\mathcal{C}}_{\boldsymbol{\mathcal{W}}}$	Speed matrix within the diagonalisation basis
$\boldsymbol{\mathcal{C}}_{\boldsymbol{\mathcal{Y}}}$	Speed matrix coupled fluid and solid pressure-velocity wave equation
$\boldsymbol{\mathcal{N}}$, $\boldsymbol{\mathcal{M}}$, $\boldsymbol{\mathcal{Q}}$, $\boldsymbol{\mathcal{R}}$, $\boldsymbol{\mathcal{S}}$	Boundary condition matrices within the diagonalisation basis

$\mathbf{\Phi}_k(Z)$	Eigenvector of $\mathcal{H}$
$\tilde{\mathbf{\Phi}}_k(Z)$	Contracted form of $\mathbf{\Phi}_k$

Notations

$\langle\cdot\rangle$	Scalar product
η_1, η_2	Constant of the scalar product
$\cdot^*$	Dimensionall field
$\hat{\cdot}$	Laplace transform
s	Laplace variable
t	Dimensionall time
τ	Dimensionless time
β, $\kappa_\pm$, γ, ξ_k	Constants
$\kappa = \frac{\kappa_-}{\kappa_+}$	Constant ratio

Appendix B. Dimensionless FSI four equations

[7] provides a derivation of well-known FSI four-equations system. From averaged mass and momentum conservation equations within fluid and solid, [7] founds the coupled hyperbolic equations for longitudinal fluid velocity W^*, pressure P^*, longitudinal solid deformation velocity $\dot{\zeta}^*$ and longitudinal stress σ^*,

$$\partial_t W^* = -\frac{1}{\rho_f}\partial_z P^*, \tag{B.1}$$

$$\partial_z W^* + \frac{1}{\rho_f c_p^2}\partial_t P^* = 2\nu_s \partial_z \dot{\zeta}^*, \tag{B.2}$$

$$\partial_t \dot{\zeta}^* = \frac{1}{\rho_s}\partial_z \sigma^*, \tag{B.3}$$

$$\partial_t \sigma^* - E\partial_z \dot{\zeta}^* = \frac{2\nu_s}{\alpha\,(2+\alpha)}\partial_t P^*, \tag{B.4}$$

where subscript * refers to dimensional quantities. The velocity perturbation W^* reference amplitude is set as W_0, so that as $W^* = W_0 W$. The pressure perturbation P^*, is known from [1]'s theory to match the dynamic pulse over-pressure so that $P^* = \rho_f c_p W_0 P$. From stress continuity at the tube wall, the

axial perturbed stress, σ^* is prescribed having the same order of magnitude as P^*, i.e. $\sigma^* = \rho_f c_p W_0 \sigma$. The axial displacement field, ζ^*, is set as $\zeta^* = \alpha \frac{\mathcal{M}}{\epsilon} R_0 \zeta$ in order to ensure both axial velocity matching at the tube's wall and the small strain and small displacement hypothesis framework. Furthermore, the physical time, t, is scaled on the advection time, $t = \frac{L}{c_p}\tau$ whilst axial longitudinal scale is set as $z = LZ$. Using these scaling within (B.1)-(B.4), leads to (7).

Appendix C. Resolution of the constitutive ODE in $a_k(\tau)$

Let's consider the ODE

$$\left(\partial_\tau^2 + \lambda_k^2\right) a_k(\tau) = -\frac{\langle \partial_\tau^2 \boldsymbol{\mathcal{Y}}_p, \tilde{\boldsymbol{\Phi}}_k(Z)\rangle}{\|\tilde{\boldsymbol{\Phi}}_k\|}, \tag{C.1}$$

and its initial conditions

$$a_k(0) = -\frac{\langle \boldsymbol{\mathcal{Y}}_p(Z,0), \tilde{\boldsymbol{\Phi}}_k(Z)\rangle}{\|\tilde{\boldsymbol{\Phi}}_k\|}, \text{ and, } \partial_\tau a_k(0) = -\frac{\langle \partial_\tau \boldsymbol{\mathcal{Y}}_p(Z,0), \tilde{\boldsymbol{\Phi}}_k(Z)\rangle}{\|\tilde{\boldsymbol{\Phi}}_k\|}. \tag{C.2}$$

A Laplace transform, hereby denoted $\mathcal{L}$, approach is employed to solve (C.1). Introducing s, the conjugate variable of t and setting up hat notation for Laplace variables yields

$$\begin{aligned}\left(s^2 + \lambda_k^2\right) \hat{a}(s) - s a_k(0) - \partial_\tau a_k(0) = -s^2 \frac{\langle \hat{\boldsymbol{\mathcal{Y}}}_p, \tilde{\boldsymbol{\Phi}}_k(Z)\rangle}{\|\tilde{\boldsymbol{\Phi}}_k\|} \\ + \frac{s\langle \boldsymbol{\mathcal{Y}}_p(Z,0), \tilde{\boldsymbol{\Phi}}_k(Z)\rangle + \langle \partial_\tau \boldsymbol{\mathcal{Y}}_p(Z,0), \tilde{\boldsymbol{\Phi}}_k(Z)\rangle}{\|\tilde{\boldsymbol{\Phi}}_k\|}.\end{aligned} \tag{C.3}$$

Inovking (C.2) reads to

$$\hat{a}_k(s) = \lambda_k^2 \frac{\langle \hat{\boldsymbol{\mathcal{Y}}}_p, \tilde{\boldsymbol{\Phi}}_k(Z)\rangle}{(s^2 + \lambda_k^2)\|\tilde{\boldsymbol{\Phi}}_k\|} - \frac{\langle \hat{\boldsymbol{\mathcal{Y}}}_p, \tilde{\boldsymbol{\Phi}}_k(Z)\rangle}{\|\tilde{\boldsymbol{\Phi}}_k\|}. \tag{C.4}$$

Since $\mathcal{L}\left(\sin\left(\lambda_k \tau\right)\right) = \frac{\lambda_k}{s^2 + \lambda_k^2}$, the use of convolution theorem finally results in

$$a_k(\tau) = \lambda_k \int_0^\tau \frac{\langle \boldsymbol{\mathcal{Y}}_p, \tilde{\boldsymbol{\Phi}}_k(Z)\rangle(t) \sin\left(\lambda_k\left[\tau - t\right]\right) dt}{\|\tilde{\boldsymbol{\Phi}}_k\|} - \frac{\langle \boldsymbol{\mathcal{Y}}_p, \tilde{\boldsymbol{\Phi}}_k(Z)\rangle}{\|\tilde{\boldsymbol{\Phi}}_k\|}. \tag{C.5}$$

Appendix D. Derivation of $\tilde{\mathbf{\Phi}}_k(Z)$ in configuration (i)

Let's focus on the first configuration boundary matrices (50) along with the homogeneous system upon $(\mathbf{\Phi}_k(0), \partial_Z \mathbf{\Phi}_k(0))^T$ in (33). Introducing the fourth unknown column vector

$$\begin{pmatrix} \mathbf{\Phi}_k(0) \\ \partial_Z \mathbf{\Phi}_k(0) \end{pmatrix} = \left(\phi_k^-, \phi_k^+, \partial_Z \phi_k^-, \partial_Z \phi_k^+\right)^T \tag{D.1}$$

yields

$$\begin{pmatrix} 1 & \frac{\beta c_-}{c_+} & 0 & 0 \\ 0 & 0 & \frac{1}{c_-} & \frac{1}{c_+} \\ -\frac{\lambda_k \sin\left(\frac{\lambda_k}{c_-}\right)}{c_-} & -\frac{\lambda_k \beta c_- \sin\left(\frac{\lambda_k}{c_+}\right)}{c_+^2} & \frac{\cos\left(\frac{\lambda_k}{c_-}\right)}{c_-} & \frac{\beta c_- \cos\left(\frac{\lambda_k}{c_+}\right)}{c_+^2} \\ -\frac{\lambda_k \sin\left(\frac{\lambda_k}{c_-}\right)}{c_-} & -\frac{\lambda_k \sin\left(\frac{\lambda_k}{c_+}\right)}{c_+} & \frac{\cos\left(\frac{\lambda_k}{c_-}\right)}{c_-} & \frac{\cos\left(\frac{\lambda_k}{c_+}\right)}{c_+} \end{pmatrix} \begin{pmatrix} \phi_k^- \\ \phi_k^+ \\ \partial_Z \phi_k^- \\ \partial_Z \phi_k^+ \end{pmatrix} = \mathbf{0}. \tag{D.2}$$

A non homogeneous solution of this linear system follows from re-organizing the last two lines of (D.2) and achieves in

$$\begin{pmatrix} \phi_k^+ \\ \partial_Z \phi_k^- \\ \partial_Z \phi_k^+ \end{pmatrix} = \phi_k^- \begin{pmatrix} -\frac{c_-}{\beta c_-} \\ \frac{\lambda_k}{c_-} \tan\left(\frac{\lambda_k}{c_-}\right) \\ -\frac{c_+}{\beta c_-} \frac{\lambda_k}{c_+} \tan\left(\frac{\lambda_k}{c_+}\right) \end{pmatrix}. \tag{D.3}$$

The use of (D.3) within the equations set (30)-(32) in case of a separate pressure - velocity boundary conditions (i.e. $\mathbf{T} \equiv \mathbf{T}_s$ such as transfer matrices order are divided by two) results in

$$\mathbf{\Phi}_k(Z) = \phi_k^- \begin{pmatrix} \cos\left(\frac{\lambda_k Z}{c_-}\right) + \tan\left(\frac{\lambda_k}{c_-}\right) \sin\left(\frac{\lambda_k Z}{c_-}\right) \\ -\frac{c_+}{\beta c_-} \left(\cos\left(\frac{\lambda_k Z}{c_+}\right) + \tan\left(\frac{\lambda_k}{c_+}\right) \sin\left(\frac{\lambda_k Z}{c_+}\right)\right) \end{pmatrix}, \tag{D.4}$$

so that the reduced eigenfunction form $\tilde{\mathbf{\Phi}}_k(Z)$ in (35), follows

$$\tilde{\mathbf{\Phi}}_k(Z) = \begin{pmatrix} \cos\left(\frac{\lambda_k Z}{c_-}\right) + \tan\left(\frac{\lambda_k}{c_-}\right) \sin\left(\frac{\lambda_k Z}{c_-}\right) \\ -\frac{c_+}{\beta c_-} \left(\cos\left(\frac{\lambda_k Z}{c_+}\right) + \tan\left(\frac{\lambda_k}{c_+}\right) \sin\left(\frac{\lambda_k Z}{c_+}\right)\right) \end{pmatrix}. \tag{D.5}$$

Appendix E. $\nu_s = 0$ limit of the first configuration (Cf. Fig.1a)

We hereby consider the $\nu_s = 0$ limit of our solution and compare it with the one of [31] (only its leading order).

Appendix E.1. Wave speed mode $c_\pm$ for $\nu_s \ll 1$

Using c_p^2, c_s^2 and $\mathcal{C}_s^2$ definitions (2), one can find

$$\mathcal{C}_s^2 = \mu_a + \mu_b \nu_s + \mu_c \nu_s^2, \tag{E.1}$$

with

$$\mu_a = \mathcal{D}\left(2 + \frac{E}{\mathcal{K}_T} + \frac{4}{\alpha(2+\alpha)}\right), \tag{E.2}$$

$$\mu_b = 2\mathcal{D}, \tag{E.3}$$

$$\mu_c = -\frac{4\mathcal{D}}{\alpha(2+\alpha)}. \tag{E.4}$$

Furthermore, accordingly to (15), the wave speed $c_\pm$ reads

$$c_\pm^2 = \frac{1 + \mu_a + \nu_s\mu_b \pm (\mu_a - 1)\sqrt{1 + \frac{\nu_s\mu_b}{\mu_a - 1} + \frac{\nu_s^2(\mu_b^2 + 4\mu_c)}{(\mu_a-1)^2}}}{2}, \tag{E.5}$$

so that Taylor expanding (E.5) in the $\nu_s \ll 1$ results in

$$\left(c_+^2 - c_-^2\right) = (\mu_a - 1) + \frac{\mu_b}{2}\nu_s + O(\nu_s^2), \tag{E.6}$$

$$c_+ = \sqrt{\mu_a} + \frac{3\mu_b}{8\sqrt{m u_a}}\nu_s + O(\nu_s^2), \tag{E.7}$$

$$c_- = 1 + \frac{\mu_b}{8}\nu_s + O(\nu_s^2). \tag{E.8}$$

Appendix E.2. Spectrum of configuration (i) in the $\nu_s = 0$ limit

Using β definition (49) and regarding (E.7)-(E.8) in the limit $\nu_s \to 0$, the spectrum transcendental equation (56) reduces to,

$$\cos(\lambda_k)\sin\left(\frac{\lambda_k}{\sqrt{\mu_a}}\right) = 0. \tag{E.9}$$

The solution of which are [31]'s spectrum union pure elastic-wave eigenvalues,

$$\lambda_k = \left\{\pi\left(\frac{1}{2} + k\right)\right\} \cup \left\{\pi\sqrt{\mu_a}\,(1+k)\right\}. \tag{E.10}$$

Appendix E.3. Pressure solution of configuration (i) in the $\nu_s = 0$ limit

The pressure field for configuration (i) is obtained combining (59) with the change of basis (17)-(19) and achieves in

$$P(Z,\tau) = \frac{c_+^2-1}{(c_+^2-c_-^2)} \sum_{\mathcal{S}_\mathcal{P}} \frac{\langle Z \begin{pmatrix} 1 \\ -1 \end{pmatrix}, \tilde{\mathbf{\Phi}}_k(Z)\rangle}{\|\tilde{\mathbf{\Phi}}_k(Z)\|^2} \left(\tilde{\mathbf{\Phi}}_k(Z)\cdot \mathbf{e}_1\right) \lambda_k \sin\left(\lambda_k \tau\right) + \frac{c_-^2-1}{(c_+^2-c_-^2)} \sum_{\mathcal{S}_\mathcal{P}} \frac{\langle Z \begin{pmatrix} 1 \\ -1 \end{pmatrix}, \tilde{\mathbf{\Phi}}_k(Z)\rangle}{\|\tilde{\mathbf{\Phi}}_k(Z)\|^2} \left(\tilde{\mathbf{\Phi}}_k(Z)\cdot \mathbf{e}_2\right) \lambda_k \sin\left(\lambda_k \tau\right). \quad \text{(E.11)}$$

Using β in (49), $\tilde{\mathbf{\Phi}}_k(Z)$ in (57), $\|\tilde{\mathbf{\Phi}}_k(Z)\|^2$ in (60) and $\langle Z\binom{1}{-1}, \tilde{\mathbf{\Phi}}_k(Z)\rangle$ in (61) leads to

$$\begin{aligned}
&\frac{c_\pm^2-1}{(c_+^2-c_-^2)} \frac{\langle Z\binom{1}{-1}, \tilde{\mathbf{\Phi}}_k(Z)\rangle}{\|\tilde{\mathbf{\Phi}}_k(Z)\|^2} \left(\tilde{\mathbf{\Phi}}_k(Z)\cdot \mathbf{e}_{\substack{1\\2}}\right) = \\
&\pm \frac{c_-^2-1}{(c_+^2-c_-^2)} \frac{2c_+^2 \cos\left(\frac{\lambda_k}{c_+}\right)\cos\left(\frac{\lambda_k}{c_-}\right)\left(\cos\left(\frac{\lambda_k}{c_+}\right)-\cos\left(\frac{\lambda_k}{c_-}\right)\right)}{\lambda_k^2\left(\frac{c_+^2}{c_-^2}\frac{c_-^2-1}{c_+^2-1}\cos^2\left(\frac{\lambda_k}{c_+}\right)-\cos^2\left(\frac{\lambda_k}{c_-}\right)\right)} \cos\left(\frac{\lambda_k}{c_\mp} Z\right) \\
&\pm \frac{c_-^2-1}{(c_+^2-c_-^2)} \frac{2c_+^2 \cos\left(\frac{\lambda_k}{c_\pm}\right)\left(\cos\left(\frac{\lambda_k}{c_+}\right)-\cos\left(\frac{\lambda_k}{c_-}\right)\right)}{\lambda_k^2\left(\frac{c_+^2}{c_-^2}\frac{c_-^2-1}{c_+^2-1}\cos^2\left(\frac{\lambda_k}{c_+}\right)-\cos^2\left(\frac{\lambda_k}{c_-}\right)\right)} \sin\left(\frac{\lambda_k}{c_\mp}\right)\sin\left(\frac{\lambda_k}{c_\mp} Z\right),
\end{aligned} \quad \text{(E.12)}$$

where upper/lower symbols $\pm$ & $\mp$ are combined with upper $\mathbf{e}_1 \equiv \binom{1}{0}$ /lower $\mathbf{e}_2 \equiv \binom{0}{1}$ symbol $\mathbf{e}_{\substack{1\\2}}$. The $\nu_s = 0$ spectrum limit (E.10) is the union of two distinct subsets, the contribution of which in (E.11) is now discussed separately.

- Fluid spectrum contribution

When $\nu_s = 0$ the fluid spectrum is $\lambda_{kF} = \pi\left(\frac{1}{2}+k\right)$. Furthermore, when $\nu_s \ll 1$, using (E.8), one finds $\cos^2\left(\frac{\lambda_{kF}}{c_-}\right) \sim O\left(\nu_s^2\right)$ and $\left(\frac{c_+^2}{c_-^2}\frac{c_-^2-1}{c_+^2-1}\cos^2\left(\frac{\lambda_{kF}}{c_+}\right)\right) \sim O\left(\nu_s\right)$. The $\nu_s \ll 1$, asymptotic behaviour of (E.12) can be obtained using

(E.6), (E.7) and (E.8) and results in

$$\frac{c_+^2-1}{\left(c_+^2-c_-^2\right)}\frac{\langle Z\left(\begin{smallmatrix}1\\-1\end{smallmatrix}\right),\tilde{\mathbf{\Phi}}_k(Z)\rangle}{\|\tilde{\mathbf{\Phi}}_k(Z)\|^2}\left(\tilde{\mathbf{\Phi}}_k(Z)\cdot\mathbf{e}_1\right) = (-1)^k\frac{2\sin\left(\lambda_{kF}Z\right)}{\lambda_{kF}^2}+O\left(\nu_s\right), \quad \text{(E.13)}$$

$$\frac{c_-^2-1}{\left(c_+^2-c_-^2\right)}\frac{\langle Z\left(\begin{smallmatrix}1\\-1\end{smallmatrix}\right),\tilde{\mathbf{\Phi}}_k(Z)\rangle}{\|\tilde{\mathbf{\Phi}}_k(Z)\|^2}\left(\tilde{\mathbf{\Phi}}_k(Z)\cdot\mathbf{e}_2\right) = O\left(\nu_s\right). \quad \text{(E.14)}$$

- Solid spectrum contribution

When $\nu_s=0$ the solid spectrum is $\lambda_{kS}=\sqrt{\mu_a}\pi\left(1+k\right)$. In this case, (E.12)'s denominators do not cancel each other so that the $\nu_s\ll 1$ behavior is trivial,

$$\frac{c_\pm^2-1}{\left(c_+^2-c_-^2\right)}\frac{\langle Z\left(\begin{smallmatrix}1\\-1\end{smallmatrix}\right),\tilde{\mathbf{\Phi}}_k(Z)\rangle}{\|\tilde{\mathbf{\Phi}}_k(Z)\|^2}\left(\tilde{\mathbf{\Phi}}_k(Z)\cdot\mathbf{e}_{\begin{smallmatrix}1\\2\end{smallmatrix}}\right) = O\left(\nu_s\right). \quad \text{(E.15)}$$

Combining (E.8)-(E.15) in (E.11), finally leads to [31]'s leading order solution

$$\lim_{\nu_s\to 0}\left(P(Z,\tau)\right) = 2\sum_{k=0}^{\infty}(-1)^k\frac{\sin\left(\lambda_{kF}Z\right)\sin\left(\lambda_{kF}\tau\right)}{\lambda_{kF}}. \quad \text{(E.16)}$$

Appendix F. Analytical analysis of $\frac{\boldsymbol{\beta c_-\kappa_-}}{\boldsymbol{c_+\kappa_+}}$

Let us set up

$$\chi=\frac{1-\frac{2\nu_s\mathcal{D}}{\alpha(2+\alpha)(c_+^2-1)}}{1-\frac{2\nu_s\mathcal{D}}{\alpha(2+\alpha)(c_-^2-1)}}, \quad \text{(F.1)}$$

so that inovking the definition of $\kappa_\pm$ in (68), it leads to

$$\frac{\kappa_-}{\chi\kappa_+}=\frac{1+\frac{2\nu_s}{c_-^2-1}}{1+\frac{2\nu_s}{c_+^2-1}}\frac{1-\frac{2\nu_s\mathcal{D}}{\alpha(2+\alpha)(c_-^2-1)}}{1-\frac{2\nu_s\mathcal{D}}{\alpha(2+\alpha)(c_+^2-1)}}. \quad \text{(F.2)}$$

Reorganising (F.2) then follows

$$\frac{\kappa_-}{\chi\kappa_+}=\left(\frac{c_+^2-1}{c_-^2-1}\right)^2\left(\frac{c_-^2-1+2\nu_s}{c_+^2-1+2\nu_s}\right)\left(\frac{c_-^2-1-\frac{2\nu_s\mathcal{D}}{\alpha(2+\alpha)}}{c_+^2-1-\frac{2\nu_s\mathcal{D}}{\alpha(2+\alpha)}}\right). \quad \text{(F.3)}$$

Developping the term

$$\left(c_\pm^2-1+2\nu_s\right)\left(c_\pm^2-1-\frac{2\nu_s\mathcal{D}}{\alpha(2+\alpha)}\right)=$$
$$c_\pm^4-c_\pm^2\left[1+\frac{2\nu_s\mathcal{D}}{\alpha(2+\alpha)}+1-2\nu_s\right]+1+\frac{2\nu_s\mathcal{D}}{\alpha(2+\alpha)}-2\nu_s-\frac{4\nu_s^2\mathcal{D}}{\alpha(2+\alpha)}, \quad \text{(F.4)}$$

whilst using relation (14) for dimensionless wave speeds in (F.4) leads to

$$\left(c_{\pm}^2-1+2\nu_s\right)\cdot\left(c_{\pm}^2-1-\frac{2\nu_s\mathcal{D}}{\alpha(2+\alpha)}\right)= \\ -\left(c_{\pm}^2-1\right)\left[1+\frac{2\nu_s\mathcal{D}}{\alpha(2+\alpha)}-2\nu_s-\mathcal{C}_s^2-\frac{4\nu_s^2\mathcal{D}}{\alpha(2+\alpha)}\right], \quad \text{(F.5)}$$

so that using β definition (49) within (F.3) simplifies to

$$\frac{\kappa_-}{\chi\kappa_+}=\frac{c_+^2-1}{c_-^2-1}=\frac{c_+}{\beta c_-}. \quad \text{(F.6)}$$

Finally, one finds

$$\frac{c_-\beta\kappa_-}{c_+\kappa_+}=\chi=\frac{1-\frac{2\nu_s\mathcal{D}}{\alpha(2+\alpha)(c_+^2-1)}}{1-\frac{2\nu_s\mathcal{D}}{\alpha(2+\alpha)(c_-^2-1)}}. \quad \text{(F.7)}$$

Appendix G. Derivation of $\tilde{\mathbf{\Phi}}_k(Z)$ for second configuration (Cf. Fig.1b)

Let's focus on the second configuration boundary matrices (69) along with the homogeneous system upon $(\mathbf{\Phi}_k(0),\partial_Z\mathbf{\Phi}_k(0))^T$ in (33). Using (D.1), it follows

$$\begin{pmatrix} 1 & \frac{\beta c_-}{c_+} & 0 & 0 \\ 0 & 0 & \frac{1}{c_-} & \frac{1}{c_+} \\ -\frac{\lambda_k\kappa_-\sin\left(\frac{\lambda_k}{c_-}\right)}{c_-} & -\frac{\lambda_k\kappa_+\sin\left(\frac{\lambda_k}{c_+}\right)}{c_+} & \kappa_-\cos\left(\frac{\lambda_k}{c_-}\right) & \kappa_+\cos\left(\frac{\lambda_k}{c_+}\right) \\ \cos\left(\frac{\lambda_k}{c_-}\right) & \frac{\beta c_-\kappa_-}{c_+\kappa_+}\cos\left(\frac{\lambda_k}{c_+}\right) & \frac{c_-\sin\left(\frac{\lambda_k}{c_-}\right)}{\lambda_k} & \frac{\beta c_-\kappa_-\sin\left(\frac{\lambda_k}{c_+}\right)}{\kappa_+} \end{pmatrix}\begin{pmatrix}\phi_k^-\\ \phi_k^+\\ \partial_Z\phi_k^-\\ \partial_Z\phi_k^+\end{pmatrix}=\mathbf{0}. \quad \text{(G.1)}$$

Using the first two lines simplifies to

$$\begin{pmatrix} -\frac{\lambda_k}{c_-}\left[\sin\left(\frac{\lambda_k}{c_-}\right)-\frac{\kappa_+}{\beta\kappa_-}\sin\left(\frac{\lambda_k}{c_+}\right)\right] & \cos\left(\frac{\lambda_k}{c_-}\right)-\frac{\kappa_+}{\kappa_-}\cos\left(\frac{\lambda_k}{c_+}\right) \\ \cos\left(\frac{\lambda_k}{c_-}\right)-\frac{\kappa_-}{\kappa_+}\cos\left(\frac{\lambda_k}{c_+}\right) & \frac{c_-}{\lambda_k}\left[\sin\left(\frac{\lambda_k}{c_-}\right)-\frac{\beta\kappa_-}{\kappa_+}\sin\left(\frac{\lambda_k}{c_+}\right)\right] \end{pmatrix}\begin{pmatrix}\phi_k^-\\ \partial_Z\phi_k^-\end{pmatrix}=\mathbf{0}, \quad \text{(G.2)}$$

and

$$\phi_k^+=-\frac{c_+}{\beta c_-}\phi_k^- \quad \text{, and, } \quad \partial_Z\phi_k^+=-\frac{c_+}{c_-}\partial_Z\phi_k^-. \quad \text{(G.3)}$$

Let's check out the following relation

$$\frac{\sin\left(\frac{\lambda_k}{c_-}\right)-\frac{\kappa_+}{\beta\kappa_-}\sin\left(\frac{\lambda_k}{c_+}\right)}{\cos\left(\frac{\lambda_k}{c_-}\right)-\frac{\kappa_+}{\kappa_-}\cos\left(\frac{\lambda_k}{c_+}\right)}=-\frac{\cos\left(\frac{\lambda_k}{c_-}\right)-\frac{\kappa_-}{\kappa_+}\cos\left(\frac{\lambda_k}{c_+}\right)}{\sin\left(\frac{\lambda_k}{c_-}\right)-\frac{\beta\kappa_-}{\kappa_+}\sin\left(\frac{\lambda_k}{c_+}\right)}. \tag{G.4}$$

The (G.4) holds only if

$$\sin^2\left(\frac{\lambda_k}{c_-}\right)-\left[\frac{\beta\kappa_-}{\kappa_+}+\frac{\kappa_+}{\beta\kappa_-}\right]\sin\left(\frac{\lambda_k}{c_-}\right)\sin\left(\frac{\lambda_k}{c_+}\right)+\sin^2\left(\frac{\lambda_k}{c_+}\right)= \\ -\cos^2\left(\frac{\lambda_k}{c_-}\right)+\left[\frac{\kappa_-}{\kappa_+}+\frac{\kappa_+}{\kappa_-}\right]\cos\left(\frac{\lambda_k}{c_-}\right)\cos\left(\frac{\lambda_k}{c_+}\right)-\cos^2\left(\frac{\lambda_k}{c_+}\right), \tag{G.5}$$

or otherwise

$$\frac{1}{\beta}\left[1+\left(\frac{\kappa_-\beta}{\kappa_+}\right)^2\right]\sin\left(\frac{\lambda_k}{c_-}\right)\sin\left(\frac{\lambda_k}{c_+}\right)+\left[1+\left(\frac{\kappa_-}{\kappa_+}\right)^2\right]\cos\left(\frac{\lambda_k}{c_-}\right)\cos\left(\frac{\lambda_k}{c_+}\right) \\ =\frac{2\kappa_-}{\kappa_+}, \tag{G.6}$$

which is the transcendent spectrum (73) satisfied by λ_k. Introducing ξ_k

$$\xi_k=\frac{\sin\left(\frac{\lambda_k}{c_-}\right)-\frac{\kappa_+}{\beta\kappa_-}\sin\left(\frac{\lambda_k}{c_+}\right)}{\cos\left(\frac{\lambda_k}{c_-}\right)-\frac{\kappa_+}{\kappa_-}\cos\left(\frac{\lambda_k}{c_+}\right)}, \tag{G.7}$$

thus leads to

$$\partial_Z\phi_k^-=\frac{\lambda_k\xi_k}{c_-}\phi_k^-. \tag{G.8}$$

Finally, using the expression of ϕ_k^+, $\partial_Z\phi_k^+$, $\partial_Z\phi_k^-$ versus ϕ_k^- in (G.3)-(G.8) and the equations set (30)-(32) in case of a separate pressure - velocity boundary conditions (i.e $\mathbf{T}\equiv\mathbf{T}_s$ such as transfer matrices order are divided by two) results in

$$\mathbf{\Phi}_k(Z)=\phi_k^-\left[\begin{pmatrix}\cos\left(\frac{\lambda_k}{c_-}Z\right)\\ -\frac{c_+}{\beta c_-}\cos\left(\frac{\lambda_k}{c_+}Z\right)\end{pmatrix}+\xi_k\begin{pmatrix}\sin\left(\frac{\lambda_k}{c_-}Z\right)\\ -\frac{c_+}{c_-}\sin\left(\frac{\lambda_k}{c_+}Z\right)\end{pmatrix}\right], \tag{G.9}$$

so that the reduced form of $\mathbf{\Phi}_k(Z)$, $\tilde{\mathbf{\Phi}}_k(Z)$ is consequently

$$\tilde{\mathbf{\Phi}}_k(Z)=\begin{pmatrix}\cos\left(\frac{\lambda_k}{c_-}Z\right)+\xi_k\sin\left(\frac{\lambda_k}{c_-}\right)\\ -\frac{c_+}{\beta c_-}\left[\cos\left(\frac{\lambda_k}{c_+}Z\right)+\beta\xi_k\sin\left(\frac{\lambda_k Z}{c_+}\right)\right]\end{pmatrix}. \tag{G.10}$$